INFRARED SIGNATURES OF PROTOPLANETARY DISK EVOLUTION

Kenneth Wood[1,2], C.J. Lada[2], J.E. Bjorkman[3], Scott J. Kenyon[2], Barbara Whitney[4],
Michael J. Wolff[4]
Submitted to the Astrophysical Journal

ABSTRACT

We investigate the observational signatures of a straightforward evolutionary scenario for protoplanetary disks in which the disk mass of small ($\lesssim 50\mu$m) particles decreases homologously with time, but the disk structure and stellar parameters do not change. Our goal is to identify optimal infrared spectral indicators of the existence of disks, their structure, and mass evolution that may be tested with the upcoming *SIRTF* mission. We present simulated spectral energy distributions and colors over a wide range of masses, $10^{-8}M_\odot \leq M_{\rm disk} \leq 10^{-1}M_\odot$. Our Monte Carlo radiative equilibrium techniques enable us to explore the wide range of optical depths of these disks and incorporate multiple, anisotropic dust scattering. The SED is most sensitive to disk mass in the far-IR and longer wavelengths, which is already known from millimeter and radio observations. As the disk mass decreases, the excess emission of the disk over the stellar photosphere diminishes more rapidly at the longest rather than at short wavelengths. At near-infrared wavelengths, the disk remains optically thick to stellar radiation over a wide range of disk mass, resulting in a slower decline in the SED in this spectral regime. Therefore, near-IR excesses ($K - L$) provide a robust means of detecting disks in star clusters down to $M_{\rm disk} \sim 10^{-7}M_\odot$, while the far-IR excess probes the disk mass, the caveat being that large inner disk holes can decrease the near-IR disk emission.

Varying other disk parameters (outer radius, flaring, dust size distribution) alter the SED quantitatively, but do not change our general conclusions on the evolution of SEDs and colors with the mass of small particles in the disk. Reducing the disk mass results in a clear progression in color-color diagrams with low mass disks displaying the bluest colors. We interpret color-color diagrams for Taurus-Auriga sources in the context of decreasing disk mass. Different viewing angles yield degeneracies in the color-mass relationship, but highly inclined disks are very faint and red and are readily identified in color-magnitude diagrams.

Subject headings: radiative transfer — scattering — accretion, accretion disks — ISM: dust, extinction — stars: pre-main-sequence

1. INTRODUCTION

Protoplanetary disks are primarily detected through their signature infrared excess emission relative to a stellar photosphere (e.g., Mendoza 1968; Rydgren, Strom, & Strom 1976; Cohen & Kuhi 1979; Rucinski 1985). The IR excesses arise from the reprocessing of stellar radiation and the liberation of accretion luminosity within the disk (e.g., Lynden-Bell & Pringle 1974; Adams & Shu 1986; Adams, Lada, & Shu 1987; Kenyon & Hartmann 1987; Adams, Emerson, & Fuller 1990; Lada & Adams 1992; Hillenbrand et al. 1992). At other wavelengths, disk masses and velocity structures have been measured with radio and mm interferometers (Beckwith et al. 1990; Beckwith & Sargent 1993; Koerner, Sargent, & Beckwith 1993; Koerner & Sargent 1995; Dutery et al. 1996; Wilner & Lay 2000) and more recently, high resolution *HST* observations and ground based adaptive optics and speckle imaging techniques have imaged disks via scattered light (O'Dell, Wen, & Hu 1993; Burrows et al. 1996; Stapelfeldt et al. 1998; Padgett et al. 1999; Krist et al. 2000; Cotera et al. 2001; Grady et al. 2000; Roddier et al. 1996; Koresko 1998).

The disks that are detected range in mass, structure, and formation mechanisms. Massive, optically thick, flaring circumstellar disks, $M_{\rm disk} \gtrsim 10^{-3}M_\odot$, are a natural product of the star formation process (e.g., Shu, Adams, & Lizano 1987) and are detected around pre-main sequence Classical T-Tauri stars. Low mass "debris disks" ($M_{\rm disk} \lesssim 10^{-5}M_\odot$) are detected around older main sequence stars (Backman & Paresce 1993). The dust that gives rise to the IR excesses and scattered light images of debris disks is believed to form from collisions of planetesimals within the disks.

The advent of large IR detector arrays now allows for simultaneous multiwavelength observations of large numbers of disks in star clusters (e.g., Haisch, Lada, & Lada 2000). The upcoming *SIRTF* mission will greatly increase the wavelength coverage for studying clusters, thereby enabling detailed studies of disks over a wide range in age and mass. We therefore need to know what spectral indicators are best suited for detecting disks and determining their mass evolution.

In this paper our working hypothesis is that through

[1]School of Physics & Astronomy, University of St Andrews, North Haugh, St Andrews, Kingdom of Fife, KY16 9SS, Scotland; kw25@st-andrews.ac.uk

[2]Harvard-Smithsonian Center for Astrophysics, 60 Garden Street, Cambridge, MA 02138; clada@cfa.harvard.edu; kenyon@payne.harvard.edu

[3]Ritter Observatory, Department of Physics & Astronomy, University of Toledo, Toledo, OH 43606; jon@astro.utoledo.edu

[4]Space Science Institute, 3100 Marine Street, Suite A353, Boulder, CO 80303; bwhitney@colorado.edu, wolff@colorado.edu

time the disk mass decreases but the disk structure and stellar luminosity do not change. In our models the dominant opacity source for $\lambda \lesssim 100\mu m$ is small ($\lesssim 50\mu m$) grains, so another way of stating our model is that we assume the small particle mass traces the total mass of gas + dust. The small grain mass may decrease by the accretion of disk material or coagulation and growth of large grains and rocks while the gas is either depleted or accreted onto the star keeping the gas/dust ratio constant. The recent detection of H_2 in β Pictoris' disk and the derived gas/dust ~ 100 is consistent with our assumption (Thi et al. 2001).

We investigate the observational signatures of this simple model for disk evolution and present radiative equilibrium models for a range of disk masses and viewing angles. Model spectra are compared with semi-analytic approximations for optically thick flat and flared disks and predictions are made as to what spectral regions are most sensitive to the evolution of disk mass and at what wavelengths disk detections are robust. We perform simulations for a fiducial disk structure and dust size distribution that fits the SED of the edge-on disk system HH30 IRS. (Wood et al. 2001). § 2 describes the ingredients of our models, § 3 presents our SED simulations and shows how *SIRTF* colors are sensitive to disk mass. § 4 presents models that explore variations in parameters other than disk mass and discusses alternative disk evolution models. § 5 compares our models with color-color diagrams of Taurus-Auriga sources and we summarize our findings in § 6.

2. MODELS

2.1. *Radiative Equilibrium Calculation*

Theoretical temperature distributions and emergent spectra have been calculated for T Tauri disks using a variety of techniques. These include approximations for opaque flat disks (Adams & Shu 1986; Adams, Lada, & Shu 1987; Lada & Adams 1992) and extensions of this approach to flared disks (Kenyon & Hartmann 1987; Chiang & Goldreich 1997, 1999); two dimensional radiation transfer techniques (Efstathiou & Rowan-Robinson 1991); diffusion approximations (e.g., Sonnhalter, Preibisch, & Yorke 1995; Boss & Yorke 1996); disks which are modeled as "spherical sectors" (Men'shchikov & Henning 1997); vertical structure calculations performed by dividing the disk into plane parallel annuli (Calvet et al. 1992; Bell et al. 1997; Bell 1999; D'Alessio et al. 1998, 1999); and Monte Carlo techniques (Wolf, Henning, & Stecklum 1999). Common approximations in many of the "traditional" codes are to conduct the radiation transfer in only one direction in the disk and assume the dust grains scatter radiation isotropically. Also many techniques are limited to the study of optically thick and hence massive disks.

Monte Carlo techniques are straightforward to adapt to any geometry, mass, and can accurately include polarization and multiple, anisotropic scattering. We use the Monte Carlo radiative equilibrium technique of Bjorkman & Wood (2001) which conserves energy exactly. For very optically thick disks we use our Monte Carlo technique for the upper layers of the disk (i.e., the disk "atmosphere") and a diffusion approximation for the densest midplane regions. For the most massive disks we simulate, typically less than 1% of the flux requires a diffusion treatment. More details of our adaptation of the Bjorkman & Wood

(2001) technique for simulating T Tauri disks will be presented in Bjorkman, Wood, & Whitney (2001, in preparation). An advantage of using Monte Carlo techniques for studying a range of disk masses, is that we are not restricted to one-dimensional radiation transfer and can therefore simulate SEDs of low mass optically thin disks in which radial transport of photons is important. The output of our code is the disk temperature structure (due to heating by stellar photons and accretion luminosity) and the emergent SED and polarization spectrum at a range of viewing angles. A calculation of the hydrostatic disk structure (e.g., Chiang & Goldreich 1997; D'Alessio et al. 1999) can be included in the Monte Carlo technique, but this would require an iterative scheme. At present we have not implemented such a scheme and instead perform the radiative equilibrium calculation for a fixed disk geometry.

2.2. *Disk Structure*

The determination of disk structure from fitting SEDs and scattered light images does not yield a single structure and dust size distribution that applies to all disks. Some systems are fit with passive flat disks (e.g., Adams et al. 1987; Adams et al. 1990; Miyake & Nakagwa 1995), while others require flared disks heated by starlight and accretion luminosity (e.g., Kenyon & Hartmann 1987; Burrows et al. 1996; Stapelfeldt et al. 1998). The scattered light image of the edge-on disk of HH30 IRS (Burrows et al. 1996) has for the first time allowed the vertical structure of a protoplanetary disk to be studied directly. We therefore adopt the HH30 IRS disk as our fiducial model for our SED models. A fixed disk density structure which fits the scattered light images (Burrows et al. 1996; Cotera et al. 2001) and SED (Stapelfeldt & Monetti 1999; Wood et al. 2001) of HH30 IRS is

$$\rho = \rho_0 \left(\frac{R_\star}{\varpi} \right)^\alpha \exp{-\frac{1}{2}[z/h(\varpi)]^2} \,, \qquad (1)$$

where ϖ is the radial coordinate in the disk midplane and the scale height increases with radius, $h = h_0 \left(\varpi/R_\star\right)^\beta$. For the HH30 IRS disk we adopt $\beta = 1.25$, $\alpha = 2.25$, and $h_0 = 0.017R_\star$, giving $h(100\text{AU}) = 17\text{AU}$.

In our simulations the inner edge of the disk is truncated at the dust destruction radius, R_{dust}. Assuming $T_\star = 4000\text{K}$, $R_\star = 2R_\odot$, and circumstellar dust sublimates at 1600K, then $R_{\text{dust}} \approx 8R_\star$. This is larger than the dust destruction radius for optically thin dust because the reprocessed emission from the disk provides additional heating over and above the direct stellar radiation, increasing the size of the dust destruction zone (a detailed discussion of the shape of the dust destruction region will be presented in Bjorkman et al. 2001, in preparation). In currently popular magnetic accretion models the disk is truncated at a radius R_0, which may not be equal to R_{dust}. If $R_0 < R_{\text{dust}}$ there will be a gas disk extending from R_0 to R_{dust} which may give rise to additional IR emission. Our models therefore assume that any material within R_{dust} is optically thin, which is a good approximation for low mass disks. For high mass disks the gas may be optically thick producing larger near-IR excesses.

2.3. *Adopted Circumstellar Dust Properties*

Recent modeling of HST images (Cotera et al. 2001) and the SED of HH30 IRS (Wood et al. 2001) indicates that the circumstellar dust size distribution extends to larger grain radii than typical ISM grains. This is in agreement with many other observations indicating grain growth within protoplanetary disks (e.g., Beckwith et al. 1990; Beckwith & Sargent 1991). This paper primarily investigates the effects of disk mass on the SED and adopts circumstellar dust properties that reproduce the HH30 IRS SED. The dust model (chemical composition, mathematical form for the size distribution, calculation of opacity and scattering parameters, etc) is described in Wood et al. (2001) and we only summarize the main features here. Specifically, we adopt, a size distribution

$$n(a) \ da = C_i \ a^{-p} \exp\left(-[a/a_c]^q\right) \ da \ , \qquad (2)$$

with $p = 3.5$, $q = 0.6$, $a_c = 50\mu$m, $a_{\min} = 0.01\mu$m, and $a_{\max} = 1$mm. The exponential scalelength, a_c, yields dust particle sizes extending up to and in excess of 50μm. Figure 1 shows the wavelength dependence of the opacity, scattering albedo, and Heyney-Greenstein phase function asymmetry parameter (Heyney & Greenstein 1941) for this size distribution.

Recent *Infrared Space Observatory* spectra of Herbig Ae/Be stars (e.g., Meuss et al. 2000; Chiang et al. 2001; van den Ancker et al. 2000) are now allowing the circumstellar dust chemistry to be studied. Because we adopt the dust properties of Fig. 1 for our simulations, we have not investigated the effects of different chemical compositions on the the resulting disk SEDs. How the circumstellar chemistry effects the SED is an interesting problem, but it is beyond the scope of this paper and we present models for different disk masses and the dust properties shown in Figure 1. In addition, our models do not include additional heating from transiently heated small grains (see the new radiation transfer code of Misselt et al. 2001) which is not important in the cooler Classical T Tauri stars considered in this paper.

2.4. *Energy Sources*

The energy input to the disk is from stellar photons and accretion luminosity liberated in the disk. As discussed in the previous section, we fix the disk structure for our radiation transfer simulations. Given the disk structure (Eq. 1), α disk theory determines the accretion rate for a given disk mass. Our parameterization of the disk density and accretion follows that presented in the review by Bjorkman (1997), apart from the term $\pm\sqrt{R_0/\varpi}$. The accretion rate and viscosity parameter, $\dot{M}$ and $\alpha_{\rm disk}$, are related to the disk parameters by

$$\dot{M} = \sqrt{18\pi^3} \ \alpha_{\rm disk} \ V_c \ \rho_0 \ h_0^3/R_\star \ , \qquad (3)$$

where the critical velocity $V_c = \sqrt{GM_\star/R_\star}$. The flux due to viscous disk accretion, $GM_\star\dot{M}/2R_\star$, is generated throughout the disk midplane region according to (Shakura & Sunyaev 1973, Lynden-Bell & Pringle 1974)

$$\frac{dE}{dA \, dt} = \frac{3GM_\star\dot{M}}{4\pi\varpi^3} \left[1 - \sqrt{\frac{R_\star}{\varpi}}\right] \ . \qquad (4)$$

For low mass disks, the heating due to accretion luminosity is negligible and stellar irradiation dominates the disk heating. In general we choose $\alpha_{\rm disk} = 0.01$ (Hartmann et al. 1998), but for the most massive disk we simulate this results in a very large accretion luminosity, $L_A > 0.8L_\star$. For this case $\alpha_{\rm disk}$ is adjusted so that $L_A < 0.2L_\star$ in line with recent observational determinations of accretion luminosities in classical T Tauri stars (Hartmann et al. 1998).

3. MODEL RESULTS: SEDS, COLORS

The following models use $T_\star = 4000$K, $R_\star = 2R_\odot$, $R_{\rm disk} = 100$AU, and a distance of 500pc to the system.

3.1. *SED Evolution with Disk Mass*

Figure 2 shows the effect on the SED of changing the disk mass, but keeping the disk structure fixed to that of our fiducial model. The massive optically thick disks produce SEDs that resemble that of the Kenyon & Hartmann (1987) flared disk model, aside from differences (addition of scattered light to pole-on views and silicate features) due to our inclusion of a finite albedo and non-gray opacity. The most massive disk has a very large near-IR excess due to the large accretion luminosity present in this model. The model SEDs display the characteristic features present in other simulations: large infrared excess emission, flat spectrum sources at intermediate inclinations, and double peaked spectra (optical and far-IR peaks) for very large inclinations. At large inclinations, the optical peak is due to scattered starlight as the dense disk totally obscures the star and disk emission at short wavelengths.

Reducing the disk mass has the most dramatic effect at long wavelengths with the SED rapidly declining with decreasing mass. At short wavelengths the disk remains optically thick to stellar photons over a wide range of mass so the near-IR excess is not as sensitive to mass. Figure 4 presents our models again, with the three panels showing SEDs for the range of disk masses at a given inclination. These results show similar features to the models of Men'shchikov & Henning (1997, their Fig. 12) who presented SEDs for a range of optical depths in a spherical geometry with evacuated bipolar cones.

The *SIRTF* sensitivity limits show that at a distance of 500pc very low mass disks ($M_{\rm disk} \gtrsim 10^{-6}M_\odot$) are detectable out to a wavelength of 70μm. At 25μm *SIRTF* will be sensitive to photospheric flux levels at 500pc, thus allowing for the detection of even lower mass disks. Our overall conclusion from these simulations is that near-IR excesses detect disks while far-IR excesses can be used to study their mass.

3.2. *Color Evolution with Disk Mass*

Figure 4 shows the variation of colors with disk mass for $i < 60°$. At long wavelengths we use the simulated flux at 70μm and 160μm in forming the color and have not adopted any particular color system. The colors are fairly insensitive to inclination for $i < 60°$, but see §3.3 for color-color and color-magnitude diagrams that include highly inclined disks. For a passive disk with $M_{\rm disk} = 10^{-1}M_\odot$, $\Delta(K - L) \approx 0.7$, decreasing to a fairly constant $\Delta(K-L) \approx 0.4$ for $10^{-7}M_\odot \leq M_{\rm disk} \leq 10^{-3}M_\odot$. Larger $K - L$ colors arise in massive disks where accretion

luminosity is included, $\Delta(K-L) \approx 1$ for $M_{\rm disk} = 10^{-1}M_\odot$. In our models, less massive disks do not sustain large accretion rates (see §2.3) and the $K-L$ excess is due to reprocessing of starlight. For these disks, $K-L$ is fairly insensitive to mass as the disk remains optically thick in the near-IR for masses $M_{\rm disk} \gtrsim 10^{-7}M_\odot$. Therefore ground based near-IR observations are capable of detecting very low mass disks. Again, we emphasize that this is the mass of small ($\lesssim 50\mu$m) particles which dominate the near-IR opacity.

At longer wavelengths the SED decreases with decreasing disk mass and this is reflected in the other color indexes remaining relatively flat with disk mass until the disk becomes optically thin at the waveband under study. At the longest $MIPS$ wavelength, 160μm, the $K-160$ color shows a clear progression from the most massive to least massive disk.

3.3. Color-Color and Color-Magnitude Diagrams

Figure 5 shows color-color diagrams for our model disks assuming intrinsic stellar colors from Kenyon & Hartmann (1995, Table A5). When we include all disk inclinations there are degeneracies in the color-mass parameter space, with large viewing angles generally leading to redder colors. This result differs from other investigations (e.g., Lada & Adams 1992; Kenyon, Yi, & Hartmann 1996; Meyer, Calvet, & Hillenbrand 1997) which assumed the disk emission was proportional to $\cos i$, giving the bluest colors for edge-on viewing. More detailed radiation transfer modeling shows that a simple $\cos i$ scaling does not give the correct inclination dependence for flared disk models.

The effect of changing the disk mass is not very strong in the $(K-L)/(K-N)$ diagram for $M_{\rm disk} \gtrsim 10^{-6}M_\odot$, reflecting that at short wavelengths the disks remain optically thick over a wide range of mass. The disk masses separate out more clearly in the $(K-N)/(K-70)$ diagram. Therefore color-color diagrams of large numbers of sources that compare near and far infrared colors provide a means of determining the range of disk masses within a cluster.

Figure 5 showed that inclination effects lead to a large spread in the location of different disk masses in the color-color diagrams. This leads to degeneracies in the location of different disk masses. However, Fig. 6 shows how color-magnitude diagrams can help in breaking the mass-inclination degeneracy. Placing all our disk models on color-magnitude diagrams shows that disks viewed at large inclinations occupy the lower righthand corners, i.e., highly inclined disks are faint and red.

4. SED AND COLOR DEPENDENCE ON OTHER DISK PROPERTIES

4.1. Flat Disks

The previous sections presented SEDs for disks which have the flaring parameters that fit HH30 IRS images and SED. However, other investigations indicate a variety of disk structures in Classical T Tauri stars (e.g., Kenyon & Hartmann 1987; Miyake & Nakagawa 1995; Chiang et al. 2001). To investigate the effects of flatter disks on SEDs and colors we repeated the simulations of Fig. 2 with a reduced scaleheight $h_0 = 0.003R_\star$ giving $h(100{\rm AU}) = 3$AU. The smaller scaleheight results in the disk intercepting less

stellar radiation (e.g., Kenyon & Hartmann 1987) and consequently smaller excesses and bluer colors than our models in § 3. For a given disk mass, the mm flux is unaltered, but the mid to far-IR emission is sensitive to the disk structure (Kenyon & Hartmann 1987; Chiang et al. 2001). The qualitative variation of the SEDs and colors with disk mass remains the same.

4.2. Grain Growth

In our models the dust size distribution does not change as the disk mass decreases. However, small dust grains may coagulate to form larger grains and rocks thereby altering the grain size distribution in the disk (e.g., Beckwith, Henning, & Nakagawa 2000). This will lead to changes in the wavelength dependence of the opacity. D'Alessio et al. (2001) investigated grain growth by keeping the disk mass constant and increasing the maximum grain size (effectively reducing the population of small grains) and changing the slope of the power law size distribution. For a slope $p = 3.5$, their SED models show the largest effects occur for $\lambda \gtrsim 20\mu$m, while for $p = 2.5$ (which puts more mass into larger particles) the SEDs are similar to ours in which the total disk mass decreases. SEDs arising from either a low mass disk or a massive disk with large grains may be distinguished with detailed SED modeling.

4.3. Disk Radius

Decreasing the disk radius, but keeping the mass constant results in a disk that is denser and optically thicker than our models of § 3. A smaller disk effectively removes cool material at large radii that provides the bulk of the long wavelength emission, yielding smaller far-IR and mm fluxes (e.g., Beckwith et al. 1990). The other effect of squeezing the disk into a smaller volume is an increase in the height above the midplane at which stellar photons are absorbed. This gives a geometrically thicker dust disk that can intercept more stellar photons, raising the near and mid-IR emission. The overall effects of a very small disk are to increase the wavelength at which the disk becomes optically thin yielding larger $K-L$ colors and a slower decline in the $K-180$ color with decreasing mass. The larger optical depth for small disks will lower the minimum disk mass that may be detected from $K-L$ colors. Large radius disks give the opposite of these effects: less near and mid-IR, and more far-IR and mm emission.

4.4. Inner Disk Holes and Non-homologous Disk Evolution

In order to investigate general trends, we have presented a simple model for disk evolution of protoplanetary disks in which the mass decreases homologously with time. Real disks will be more complicated than this, with the disk radius growing, changes in the flaring parameters due to dust settling, and the possibility of accretion being terminated through the opening up of large inner disk holes and gaps, resulting in "inside-out" evolution. Current data does not provide much support for the existence of large holes in protoplanetary disks: if they do not show near-IR excesses, mid-IR and mm excesses are usually absent also (Stassun et al. 2001, Haisch, Lada & Lada 2001a), but there are some exceptions notably GM Aur (Koerner, Sargent, & Beckwith 1993). $SIRTF$ should be able to distinguish

between low mass protoplanetary disks, whose mass has evolved homologously (without creating large inner holes), and disks which have evolved by creating large inner holes and thus directly test the inside-out disk clearing scenario.

Debris disks often exhibit large inner holes or a ring-like structure (e.g., Koerner et al. 1998; Jayawardhana et al. 1998; Schneider et al. 1999). However, debris disks are not likely to be protoplanetary disks that have evolved large inner holes. Debris disks are sufficiently old that the dust in them is not remnant protoplanetary material but instead is created and continually replenished by collisions between planetessimals formed previously in the disk. Moreover, protoplanetary disks which simply evolve from the inside out by clearing large inner holes (but otherwise maintaining their initial structure), will still contain large reservoirs of material in their outer regions and thus should be considerably more massive than debris disks.

5. COMPARISON TO OBSERVATIONS: DISK MASSES IN TAURUS-AURIGA

Observations at mm and radio wavelengths, where the disk is optically thin, provide the best probe of disk mass (e.g., Beckwith et al. 1990). When such data is not available our models show that far-IR, and in certain circumstances even mid-IR data, can provide another means of probing disk mass (if the disks are not too massive and optically thick). For example, Kenyon & Hartmann (1995) presented a compilation of optical through far-IR observations of Taurus-Auriga sources and noted a pronounced gap in the $K - N$ distribution between the bluest Class II and the reddest Class III sources. Figure 7 shows the $(K - L)/(K - N)$ color-color diagram for the Taurus-Auriga sources along with our face-on model colors for various disk masses. In the context of our models, the gap in the $K - N$ distribution corresponds to disks with $M_{\rm disk} \lesssim 10^{-6} M_\odot$ and indicates that there are few circumstellar disks with masses between 10^{-6} and 10^{-8} $M_\odot$ in the Taurus-Auriga cloud (of course, this disk mass does not include rocks and planets). This, in turn, could be interpreted to indicate that once the disk mass falls below $\sim 10^{-6} M_\odot$ the timescale for clearing the remaining material in the inner ($\lesssim 5 - 10$AU) disk is very rapid.

6. SUMMARY

We have investigated the observational signatures of an evolutionary model in which the disk mass decreases homologously, but the disk structure and stellar parameters remain constant with time. Our main conclusions are:

- *Near-IR observations detect disks.* Disks remain optically thick in the near-IR over a wide range of disk mass resulting in measurable $K-L$ excesses for disks down to $M_{\rm disk} \sim 10^{-7} M_\odot$. This corresponds to a dust mass of $M_{\rm dust} \sim 10^{-9} M_\odot$.

- *Mid-IR observations probe disk structure.* Observations in the $20 \mu{\rm m} \lesssim \lambda \lesssim 100 \mu{\rm m}$ range are sensitive to the disk flaring parameters and are crucial for determining the degree of dust settling.

- *Far-IR most sensitive to disk mass.* The far-IR emission decreases rapidly with disk mass resulting in a strong correlation between $K - 160$ and disk mass. Our simulations indicate that at a distance of 500pc, *SIRTF* will be able to detect $M_{\rm disk} \gtrsim 10^{-6} M_\odot$ with a 500s exposure at 70μm and even lower masses at 25μm.

- *General trends are reproduced for a range of disk parameters.* Despite degeneracies in fitting SEDs of particular sources, we find that varying the disk parameters within generally accepted limits introduces a spread in the color-mass relationship, but does not affect the general trends.

The degeneracies inherent in fitting disk models to wavelength restricted datasets illustrates that it is necessary to have full SED coverage to constrain the disk structure and dust size distribution (e.g., Men'shchikov & Henning 1997; Chiang et al. 2001; D'Alessio et al. 2001). *SIRTF*, *SMA*, and *ALMA* will provide detailed SEDs for nearby sources enabling detailed modeling of the disk mass and structure. For studies of stellar clusters, such data will not be available and mm observations, which are most sensitive to disk mass, cannot as yet achieve the required sensitivity and resolution to study low mass disks and/or distant clusters. Therefore, we must appeal to statistics and determine average properties of sources in different clusters for studying disk evolution. *SIRTF* will provide broad band colors for hundreds of sources within a given cluster, from which we can construct median colors and the spread around the median for each cluster (e.g., Haisch, Lada, & Lada 2001b). From our models it is apparent that NIR excesses detect disks, and therefore the absence of a $K - L$ excess within a cluster of a given age can determine the maximum disk lifetime. By comparing the median colors from different clusters with a spread in age (as a whole and as functions of position within the cluster), we can search for trends as a function of cluster age. Therefore, the far-IR probed by *SIRTF* may allow us to determine a timescale for disk evolution — i.e., in our homologous evolutionary model we would be able to convert the color-mass correlation to one which tracks disk mass in clusters as a function of age, analogous to the recent *ISO* analysis of debris disks by Spangler et al. (2001).

REFERENCES

Adams, F.C., Emerson, J.P., & Fuller, G.A. 1990, ApJ, 357, 606
Adams, F.C., Lada, C.J., & Shu, F.H. 1987, ApJ, 308, 788
Adams, F.C., & Shu, F.H. 1986, ApJ, 308, 836

Backman, D.E., & Paresce, F. 1993, in Protostars and Planets III, ed. E.H. Levy & J.I. Lunine (Tuscon: Univ. Arizona Press), 1253

Beckwith, S. V. W., Henning, T., & Nakagawa, Y. in "Protostars and Planets IV," eds Mannings, V., Boss, A.P.,& Russell, S. S., (Tucson: University of Arizona Press), 533

Beckwith, S.V.W., & Sargent, A.I. 1993, in Protostars & Planets III, ed. E.H. Levy & J.I. Lunine (Tucson: Univ. Arizona), 543

Beckwith, S.V.W., & Sargent, A.I. 1991, ApJ, 381, 205

Beckwith, S.V.W., Sargent, A.I., Chini, R.S., & Gusten, R. 1990, AJ, 99, 924

Bell, K.R. 1999, ApJ, 526, 411

Bell, K.R., Cassen, P.M., Klahr, H.H., & Henning, T. 1997, ApJ, 486, 372

Bjorkman, J.E., & Wood, K. 2001, ApJ, 554, 615

Bjorkman, J.E. 1997, in "Stellar Atmospheres : Theory and Observations," eds J.P. De Greve, R. Blomme, & H. Hensberge (Springer)

Boss, A.P., & Yorke, H.W. 1996, ApJ, 469, 366

Burrows, C.J., et al. 1996, ApJ, 473, 437

Calvet, N., Canto, J., Binette, L., & Raga, A.C. 1992, Rev. Mex., 24, 81

Chiang, E.I., Joung, M.K., Creech-Eakman, M.J., Qi, C., Kessler, J.E., Blake, G.A., & van Dishoeck, E.F. 2001, ApJ, 547, 1077

Chiang, E.I., & Goldreich, P. 1999, ApJ, 519, 279

Chiang, E.I., & Goldreich, P. 1997, ApJ, 490, 368

Cohen, M., & Kuhi, L.V. 1979, ApJS, 41, 743

Cotera, A.S., et al. 2001, ApJ, 556, 958

D'Alessio, P., Calvet, N., & Hartmann, L. 2001, ApJ, 553, 321

D'Alessio, P., Calvet, N., Hartmann, L., Lizano, S., & Canto, J. 1999, ApJ, 527, 893

D'Alessio, P., Canto, J., Calvet, N., & Lizano, S. 1998, ApJ, 500, 411

Dutrey, A., Guilloteau, S., Duvert, G., Prato, L., Simon, M., Schuster, K., & Menard, F. 1996, A&A, 309, 493

Efstathiou, A., & Rowan-Robinson, M. 1991, MNRAS, 252, 528

Grady, C.A., et al. 2000, ApJ, 544, 895

Haisch, K.E., Lada, E.A., & Lada, C.J. 2001a, AJ, 121, 2065

Haisch, K.E., Lada, E.A., & Lada, C.J. 2001b, ApJ, 553, L153

Haisch, K.E., Lada, E.A., & Lada, C.J. 2000, AJ, 120, 1396

Hartmann, L., Calvet, N., Gullbring, E., & D'Alessio, P. 1998, ApJ, 495, 385

Henyey, L.C., & Greenstein, J.L. 1941, ApJ, 93, 70

Hillenbrand, L.A., Strom, S.E., Vrba, F.J., & Keene, J. 1992, ApJ, 397, 613

Jayawardhana, R., Fisher, S., Hartmann, L., Telesco, C., Pina, R., & Razio, G. 1998, ApJ, 503, L79

Kenyon, S.J., Yi, I., & Hartmann, L. 1996, ApJ, 462, 439

Kenyon, S.J., & Hartmann, L. 1995, ApJS, 101, 117

Kenyon, S.J., & Hartmann, L. 1987, ApJ, 323, 714

Kim, S.H., Martin, P.G., & Hendry, P.D. 1994, ApJ, 422, 164

Koerner, D.W., Ressler, M.E., Werner, M.W., & Backman, D.E. 1998, ApJ, 505, L83

Koerner, D.W., & Sargent, A.I. 1995, AJ, 109, 2138

Koerner, D.W., Sargent, A.I., & Beckwith, S.V.W. 1993, ApJ, 408, L93

Koresko, C.D. 1998, ApJ, 507, L145

Krist, J.E., Stapelfeldt, K.R., Menard, F., Padgett, D.L., & Burrows, C.J. 2000, ApJ, 538, 793

Lada, C.J., & Adams, F.C. 1992, ApJ, 393, 728

Lynden-Bell, D., & Pringle, J.E. 1974, MNRAS, 168, 603

Mendoza, E.E. 1968, ApJ, 151, 977

Men'shchikov, A.B., & Henning, T. 1997, A&A, 318, 879

Meyer, M.R., Calvet, N., & Hillenbrand, L.A. 1997, AJ, 114, 288

Miyake, K., & Nakagawa, Y. 1995, ApJ, 441, 361

O'Dell, C.R., Wen, Z., & Hu, X. 1993, ApJ, 410, 696

Padgett, D.L., Brandner, W., Stapelfeldt, K.R., Strom, S.E., Terebey, S., & Koerner, D.W. 1999, AJ, 117, 1490

Roddier, C., Roddier, F., Northcott, M.J., Graves, J.E., Jim, K. 1996, ApJ, 463, 326

Rucinski, S.M. 1985, AJ, 90, 2321

Rydgren, A.E., Strom, S.E., & Strom, K.M. 1976, ApJS, 30, 307

Shakura, N.I., & Sunyaev, R.A. 1973, A&A, 24, 337

Schneider, G., et al. 1999, ApJ, 513, L127

Shu, F.H., Adams, F.C., & Lizano, S. 1987, ARA&A, 25, 23

Sonnhalter, C., Preibisch, T., & Yorke, H.W. 1995, A&A, 299, 144

Spangler, C., Sargent, A.I., Silverstone, M.D., Becklin, E.E., & Zuckerman, B. 2001, ApJ, in press, astro-ph/0103185

Stapelfeldt, K. R., & Moneti, A. 1999 in "The Universe as Seen by ISO", Eds. P. Cox & M. F. Kessler, ESA-SP 427, 521

Stapelfeldt, K. R., Krist, J.E., Menard, F., Bouvier, J., Padgett, D.L., & Burrows, C.J. 1998, ApJ, 502, L65

Stassun, K.G., Mathieu, R.D., Vrba, F.J., Mazeh, T., & Henden, A. 2001, AJ, 121, 1003

Thi, W.F., et al. 2001, Nature, 409, 60

Wilner, D., & Lay, O. 2000, in "Protostars and Planets IV," eds Mannings, V., Boss, A.P.,& Russell, S. S., (Tucson: University of Arizona Press), p. 509

Wolf, S., Henning, T., & Stecklum, B. 1999, A&A, 349, 839

Wood, K., Wolff, M.J., Bjorkman, J.E., & Whitney, B.A. 2001, ApJ, in press, astro-ph/0109048
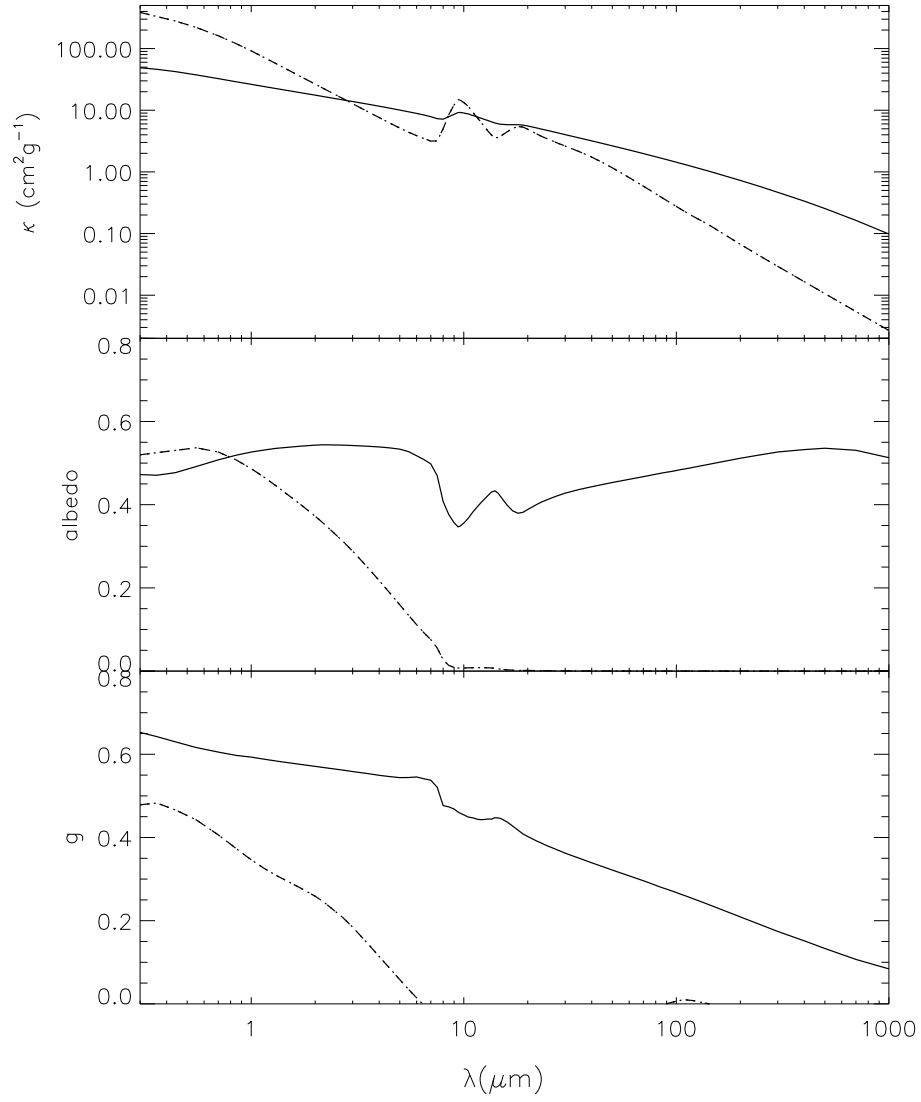
FIG. 1.— Dust parameters for a grain size distribution that fits the scattered light images and SED of HH30 IRS (solid line). The dashed lines show ISM grain parameters (Kim, Martin, & Hendry 1994). The three panels show total opacity (upper), albedo (middle), and cosine asymmetry parameter (lower).
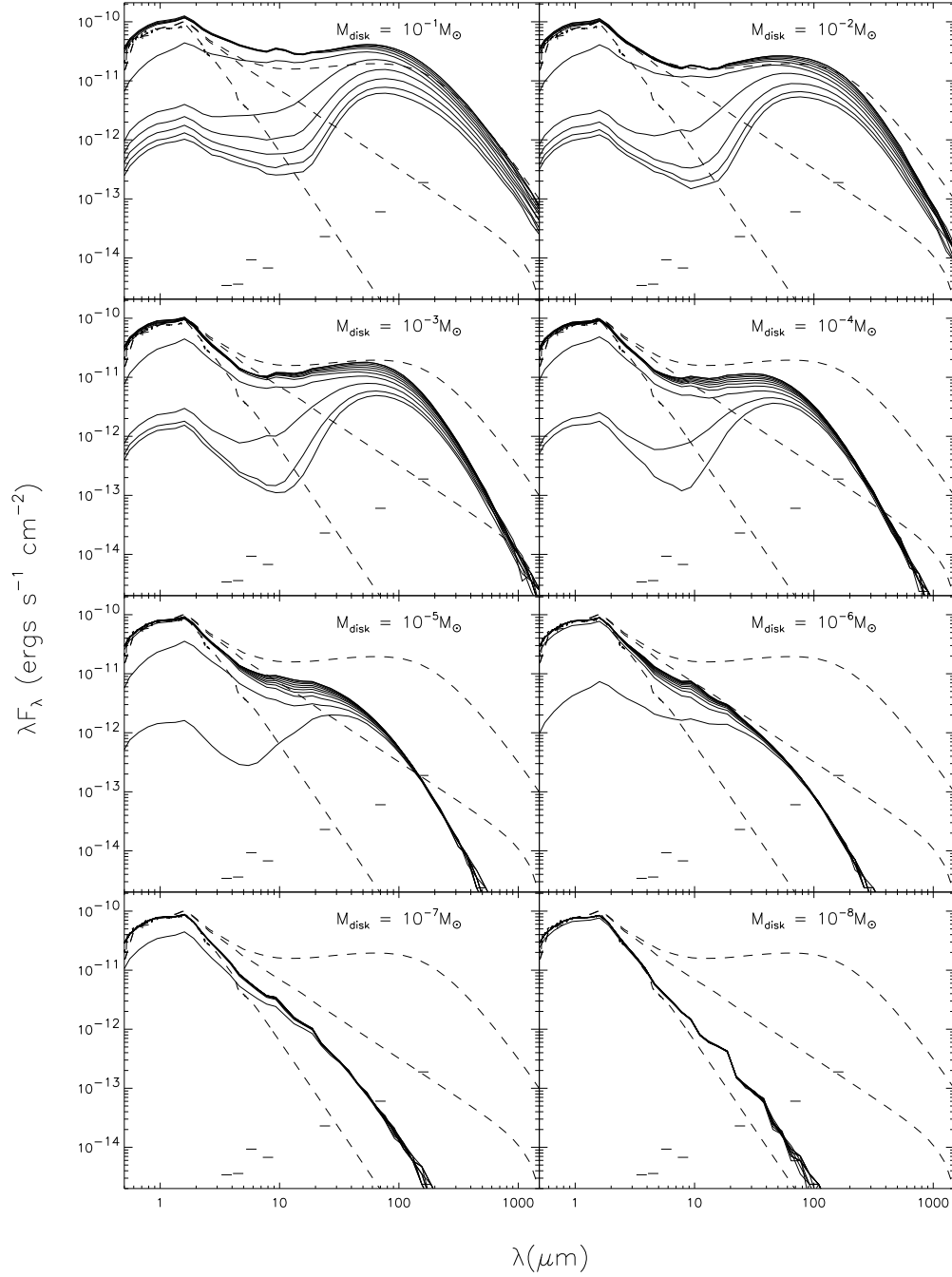
FIG. 2.— Evolution of SED with disk mass. Each panel shows model SED at ten viewing angles (evenly spaced in $\cos i$), ranging from $i = 87°$ (lowest curve) to $i = 13°$ (upper curve). Also shown are the input stellar spectrum and optically thick flat and flared reprocessing disk models. The star is assumed to be at a distance of 500pc. The short horizontal lines are 5σ *SIRTF* sensitivity limits for a 500 s exposure (http://sirtf.jpl.nasa.gov/SSC/B_Observing/SSC_B2.html).
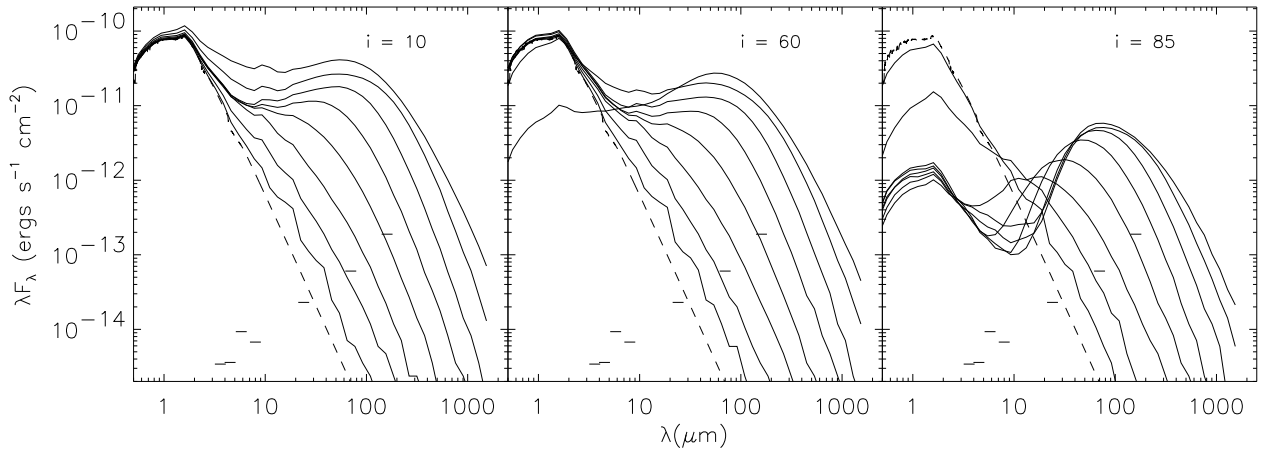
Fɪɢ. 3.— Evolution of SED with disk mass. Each panel shows model SEDs for a fixed viewing angle for the range of disk masses, $M_{\rm disk} = 10^{-8} M_\odot$ (lowest curve) to $M_{\rm disk} = 10^{-1} M_\odot$ (upper curve). Input spectrum and $SIRTF$ sensitivities are as in Fig. 3.
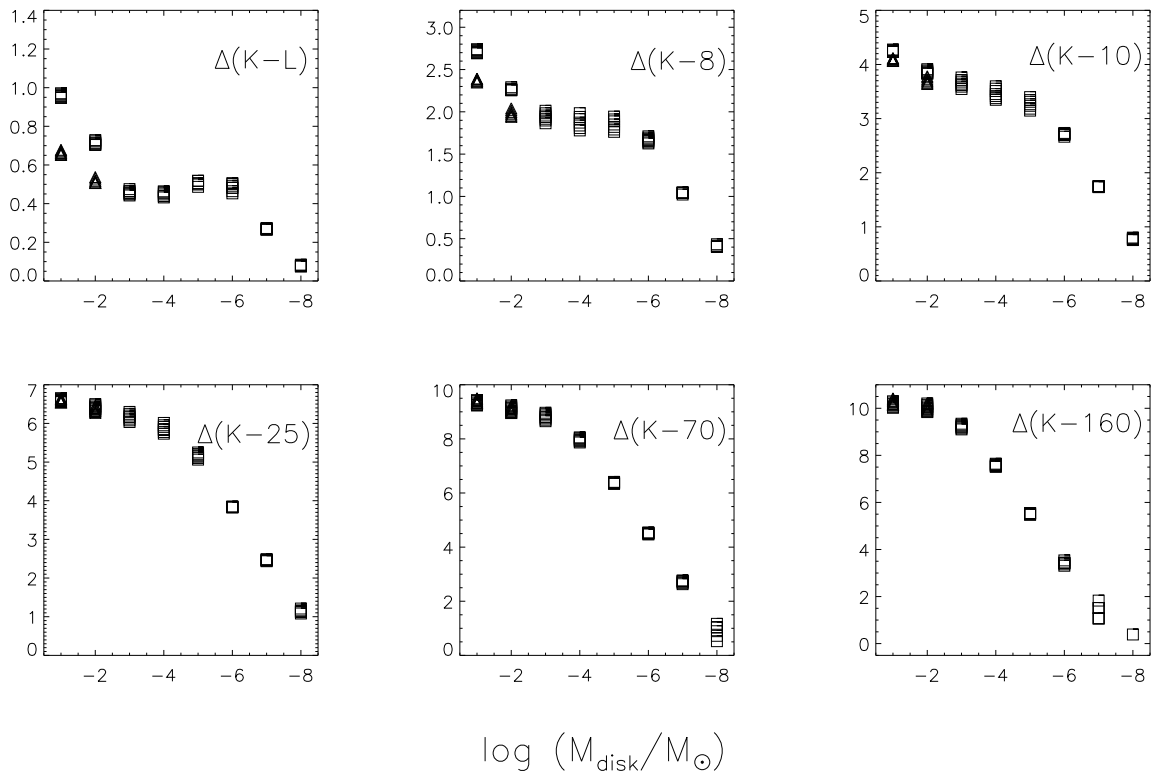
FIG. 4.— Colors as a function of disk mass for inclinations $i < 60°$. Triangles are passive disks, squares include accretion luminosity. This bottom panels show that long wavelengths are more sensitive to disk mass.
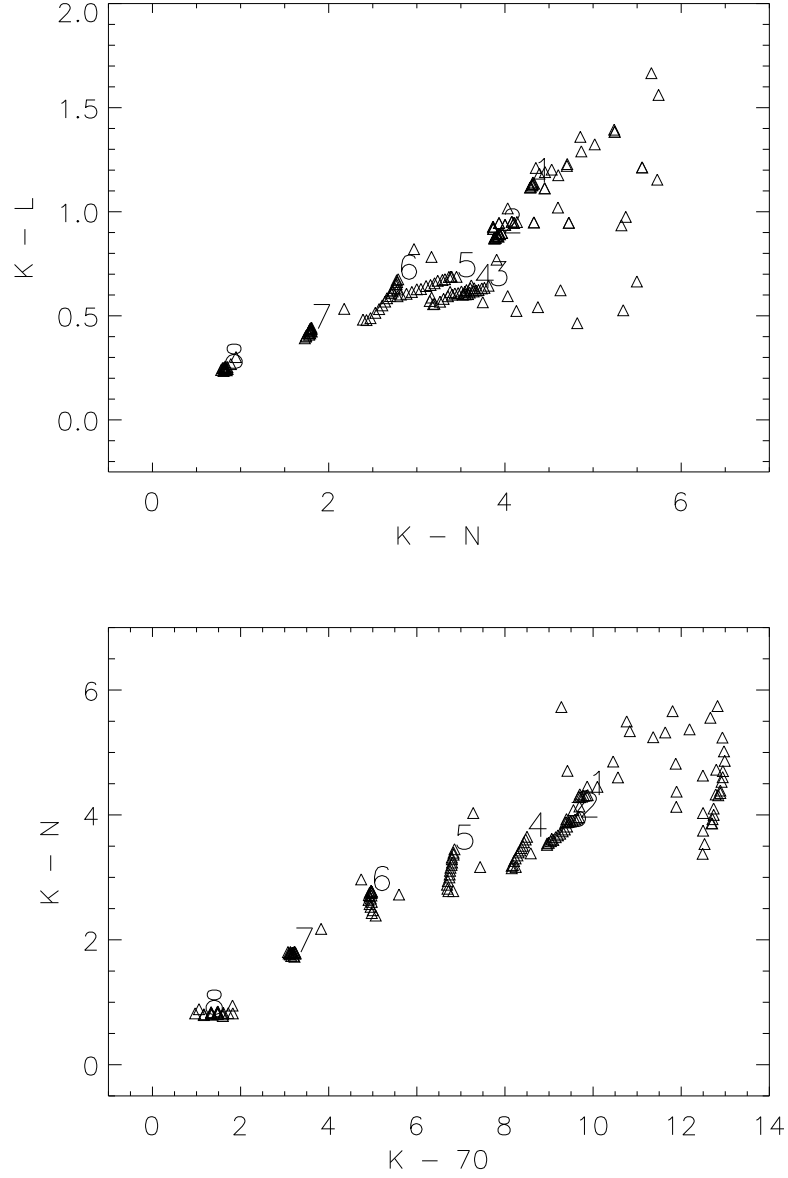
FIG. 5.— Color-color diagrams for our models. For each model we show twenty inclinations, evenly spaced in $\cos i$. The numbers are the locations of different mass disks viewed pole on, $10^{-1}M_\odot = 1$, $10^{-2}M_\odot = 2$, $10^{-3}M_\odot = 3$, etc. The very red colors are the highly inclined disks. As with Fig. 4, the bottom panel shows that long wavelength colors can distinguish a wide range of disk masses.
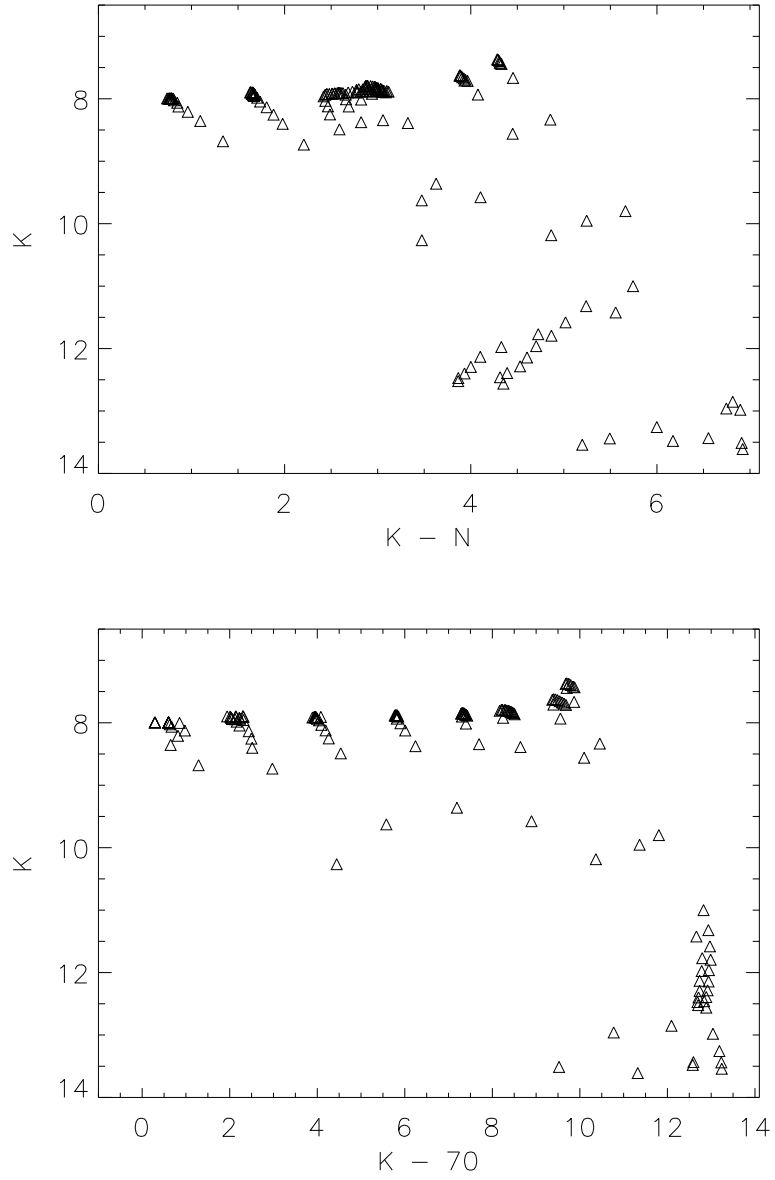
FIG. 6.— Color-magnitude diagrams for our models assuming a distance of 500pc. The edge-on disk sources are very faint and red and occupy the lower right corners of the color-magnitude diagrams.
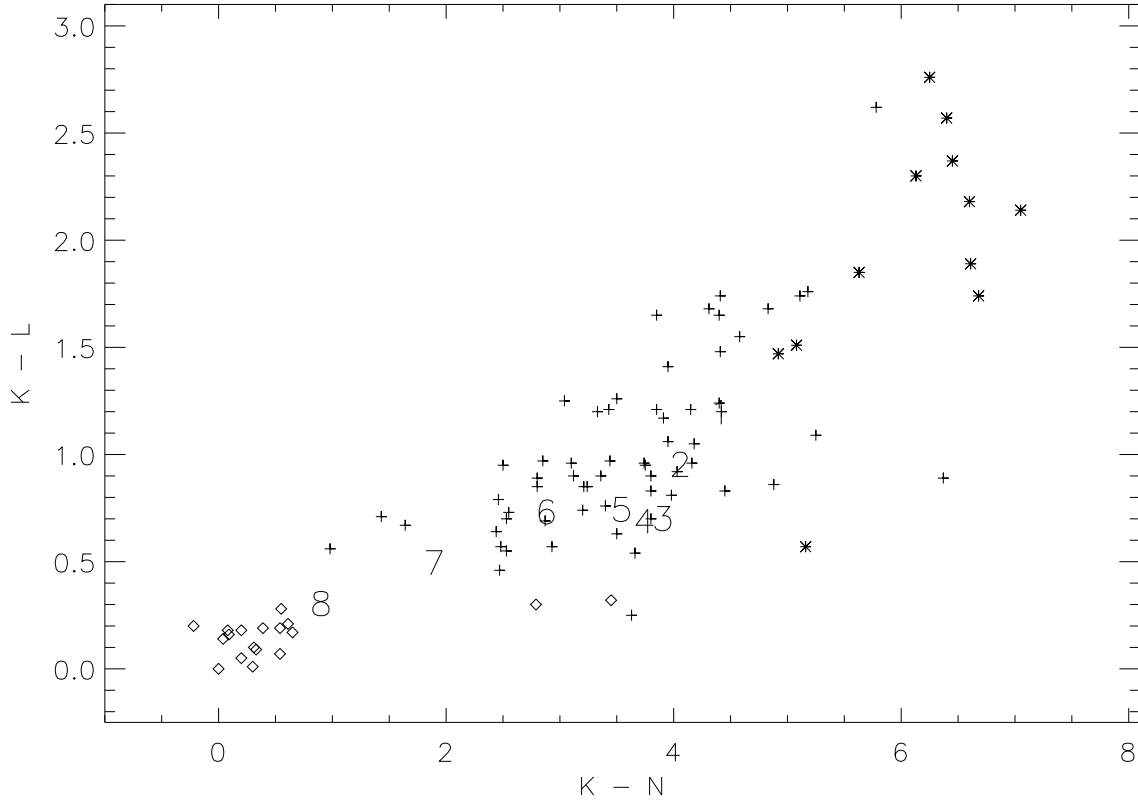
FIG. 7.— Color-color diagrams for Taurus-Auriga sources Class III (diamonds), Class II (crosses), Class I (stars). The data are taken from the Kenyon & Hartmann (1995) compilation. The numbers are our models for different mass disks viewed pole-on as in Fig. 5. The gap in the $K - N$ distribution between the Class II and Class III sources is filled in by our models having $M_{\mathrm{disk}} \lesssim 10^{-6} M_{\odot}$, which may imply that the timescale to clear $M_{\mathrm{disk}} \lesssim 10^{-6} M_{\odot}$ is very rapid.

INFRARED SIGNATURES OF PROTOPLANETARY DISK EVOLUTION

KENNETH WOOD[1,2], C.J. LADA[2], J.E. BJORKMAN[3], SCOTT J. KENYON[2], BARBARA WHITNEY[4], MICHAEL J. WOLFF[4]

ABSTRACT

We investigate the observational signatures of a straightforward evolutionary scenario for protoplanetary disks in which the disk mass of small ($\lesssim 50\mu$m) particles decreases homologously with time, but the disk structure and stellar parameters do not change. Our goal is to identify optimal infrared spectral indicators of the existence of disks, their structure, and mass evolution that may be tested with the upcoming *SIRTF* mission. We present simulated spectral energy distributions and colors over a wide range of masses, $10^{-8}M_\odot \leq M_{\rm disk} \leq 10^{-1}M_\odot$. Our Monte Carlo radiative equilibrium techniques enable us to explore the wide range of optical depths of these disks and incorporate multiple, anisotropic dust scattering. The SED is most sensitive to disk mass in the far-IR and longer wavelengths, which is already known from millimeter and radio observations. As the disk mass decreases, the excess emission of the disk over the stellar photosphere diminishes more rapidly at the longest rather than at short wavelengths. At near-infrared wavelengths, the disk remains optically thick to stellar radiation over a wide range of disk mass, resulting in a slower decline in the SED in this spectral regime. Therefore, near-IR excesses ($K - L$) provide a robust means of detecting disks in star clusters down to $M_{\rm disk} \sim 10^{-7}M_\odot$, while the far-IR excess probes the disk mass, the caveat being that large inner disk holes can decrease the near-IR disk emission.

Varying other disk parameters (outer radius, flaring, dust size distribution) alter the SED quantitatively, but do not change our general conclusions on the evolution of SEDs and colors with the mass of small particles in the disk. Reducing the disk mass results in a clear progression in color-color diagrams with low mass disks displaying the bluest colors. We interpret color-color diagrams for Taurus-Auriga sources in the context of decreasing disk mass. Different viewing angles yield degeneracies in the color-mass relationship, but highly inclined disks are very faint and red and are readily identified in color-magnitude diagrams.

Subject headings: radiative transfer — scattering — accretion, accretion disks — ISM: dust, extinction — stars: pre-main-sequence

1. INTRODUCTION

Protoplanetary disks are primarily detected through their signature infrared excess emission relative to a stellar photosphere (e.g., Mendoza 1968; Rydgren, Strom, & Strom 1976; Cohen & Kuhi 1979; Rucinski 1985). The IR excesses arise from the reprocessing of stellar radiation and the liberation of accretion luminosity within the disk (e.g., Lynden-Bell & Pringle 1974; Adams & Shu 1986; Adams, Lada, & Shu 1987; Kenyon & Hartmann 1987; Adams, Emerson, & Fuller 1990; Lada & Adams 1992; Hillenbrand et al. 1992). At other wavelengths, disk masses and velocity structures have been measured with radio and mm interferometers (Beckwith et al. 1990; Beckwith & Sargent 1993; Koerner, Sargent, & Beckwith 1993; Koerner & Sargent 1995; Dutery et al. 1996; Wilner & Lay 2000) and more recently, high resolution *HST* observations and ground based adaptive optics and speckle imaging techniques have imaged disks via scattered light (O'Dell, Wen, & Hu 1993; Burrows et al. 1996; Stapelfeldt et al. 1998; Padgett et al. 1999; Krist et al. 2000; Cotera et al. 2001; Grady et al. 2000; Roddier et al. 1996; Koresko 1998).

The disks that are detected range in mass, structure, and formation mechanisms. Massive, optically thick, flaring circumstellar disks, $M_{\rm disk} \gtrsim 10^{-3}M_\odot$, are a natural product of the star formation process (e.g., Shu, Adams, & Lizano 1987) and are detected around pre-main sequence Classical T-Tauri stars. Low mass "debris disks" ($M_{\rm disk} \lesssim 10^{-5}M_\odot$) are detected around older main sequence stars (Backman & Paresce 1993). The dust that gives rise to the IR excesses and scattered light images of debris disks is believed to form from collisions of planetesimals within the disks.

The advent of large IR detector arrays now allows for simultaneous multiwavelength observations of large numbers of disks in star clusters (e.g., Haisch, Lada, & Lada 2000). The upcoming *SIRTF* mission will greatly increase the wavelength coverage for studying clusters, thereby enabling detailed studies of disks over a wide range in age and mass. We therefore need to know what spectral indicators are best suited for detecting disks and determining their mass evolution.

In this paper our working hypothesis is that through

[1]School of Physics & Astronomy, University of St Andrews, North Haugh, St Andrews, Kingdom of Fife, KY16 9SS, Scotland; kw25@st-andrews.ac.uk

[2]Harvard-Smithsonian Center for Astrophysics, 60 Garden Street, Cambridge, MA 02138; clada@cfa.harvard.edu; kenyon@payne.harvard.edu

[3]Ritter Observatory, Department of Physics & Astronomy, University of Toledo, Toledo, OH 43606; jon@astro.utoledo.edu

[4]Space Science Institute, 3100 Marine Street, Suite A353, Boulder, CO 80303; bwhitney@colorado.edu, wolff@colorado.edu

time the disk mass decreases but the disk structure and stellar luminosity do not change. In our models the dominant opacity source for $\lambda \lesssim 100\mu m$ is small ($\lesssim 50\mu m$) grains, so another way of stating our model is that we assume the small particle mass traces the total mass of gas + dust. The small grain mass may decrease by the accretion of disk material or coagulation and growth of large grains and rocks while the gas is either depleted or accreted onto the star keeping the gas/dust ratio constant. The recent detection of H_2 in β Pictoris' disk and the derived gas/dust ~ 100 is consistent with our assumption (Thi et al. 2001).

We investigate the observational signatures of this simple model for disk evolution and present radiative equilibrium models for a range of disk masses and viewing angles. Model spectra are compared with semi-analytic approximations for optically thick flat and flared disks and predictions are made as to what spectral regions are most sensitive to the evolution of disk mass and at what wavelengths disk detections are robust. We perform simulations for a fiducial disk structure and dust size distribution that fits the SED of the edge-on disk system HH30 IRS. (Wood et al. 2001). § 2 describes the ingredients of our models, § 3 presents our SED simulations and shows how *SIRTF* colors are sensitive to disk mass. § 4 presents models that explore variations in parameters other than disk mass and discusses alternative disk evolution models. § 5 compares our models with color-color diagrams of Taurus-Auriga sources and we summarize our findings in § 6.

2. MODELS

2.1. *Radiative Equilibrium Calculation*

Theoretical temperature distributions and emergent spectra have been calculated for T Tauri disks using a variety of techniques. These include approximations for opaque flat disks (Adams & Shu 1986; Adams, Lada, & Shu 1987; Lada & Adams 1992) and extensions of this approach to flared disks (Kenyon & Hartmann 1987; Chiang & Goldreich 1997, 1999); two dimensional radiation transfer techniques (Efstathiou & Rowan-Robinson 1991); diffusion approximations (e.g., Sonnhalter, Preibisch, & Yorke 1995; Boss & Yorke 1996); disks which are modeled as "spherical sectors" (Men'shchikov & Henning 1997); vertical structure calculations performed by dividing the disk into plane parallel annuli (Calvet et al. 1992; Bell et al. 1997; Bell 1999; D'Alessio et al. 1998, 1999); and Monte Carlo techniques (Wolf, Henning, & Stecklum 1999). Common approximations in many of the "traditional" codes are to conduct the radiation transfer in only one direction in the disk and assume the dust grains scatter radiation isotropically. Also many techniques are limited to the study of optically thick and hence massive disks.

Monte Carlo techniques are straightforward to adapt to any geometry, mass, and can accurately include polarization and multiple, anisotropic scattering. We use the Monte Carlo radiative equilibrium technique of Bjorkman & Wood (2001) which conserves energy exactly. For very optically thick disks we use our Monte Carlo technique for the upper layers of the disk (i.e., the disk "atmosphere") and a diffusion approximation for the densest midplane regions. For the most massive disks we simulate, typically less than 1% of the flux requires a diffusion treatment. More details of our adaptation of the Bjorkman & Wood

(2001) technique for simulating T Tauri disks will be presented in Bjorkman, Wood, & Whitney (2001, in preparation). An advantage of using Monte Carlo techniques for studying a range of disk masses, is that we are not restricted to one-dimensional radiation transfer and can therefore simulate SEDs of low mass optically thin disks in which radial transport of photons is important. The output of our code is the disk temperature structure (due to heating by stellar photons and accretion luminosity) and the emergent SED and polarization spectrum at a range of viewing angles. A calculation of the hydrostatic disk structure (e.g., Chiang & Goldreich 1997; D'Alessio et al. 1999) can be included in the Monte Carlo technique, but this would require an iterative scheme. At present we have not implemented such a scheme and instead perform the radiative equilibrium calculation for a fixed disk geometry.

2.2. *Disk Structure*

The determination of disk structure from fitting SEDs and scattered light images does not yield a single structure and dust size distribution that applies to all disks. Some systems are fit with passive flat disks (e.g., Adams et al. 1987; Adams et al. 1990; Miyake & Nakagwa 1995), while others require flared disks heated by starlight and accretion luminosity (e.g., Kenyon & Hartmann 1987; Burrows et al. 1996; Stapelfeldt et al. 1998). The scattered light image of the edge-on disk of HH30 IRS (Burrows et al. 1996) has for the first time allowed the vertical structure of a protoplanetary disk to be studied directly. We therefore adopt the HH30 IRS disk as our fiducial model for our SED models. A fixed disk density structure which fits the scattered light images (Burrows et al. 1996; Cotera et al. 2001) and SED (Stapelfeldt & Monetti 1999; Wood et al. 2001) of HH30 IRS is

$$\rho = \rho_0 \left(\frac{R_\star}{\varpi} \right)^\alpha \exp -\frac{1}{2}[z/h(\varpi)]^2 \, , \qquad (1)$$

where ϖ is the radial coordinate in the disk midplane and the scale height increases with radius, $h = h_0 \left(\varpi/R_\star \right)^\beta$. For the HH30 IRS disk we adopt $\beta = 1.25$, $\alpha = 2.25$, and $h_0 = 0.017R_\star$, giving $h(100\text{AU}) = 17\text{AU}$.

In our simulations the inner edge of the disk is truncated at the dust destruction radius, R_{dust}. Assuming $T_\star = 4000\text{K}$, $R_\star = 2R_\odot$, and circumstellar dust sublimates at 1600K, then $R_{\text{dust}} \approx 8R_\star$. This is larger than the dust destruction radius for optically thin dust because the reprocessed emission from the disk provides additional heating over and above the direct stellar radiation, increasing the size of the dust destruction zone (a detailed discussion of the shape of the dust destruction region will be presented in Bjorkman et al. 2001, in preparation). In currently popular magnetic accretion models the disk is truncated at a radius R_0, which may not be equal to R_{dust}. If $R_0 < R_{\text{dust}}$ there will be a gas disk extending from R_0 to R_{dust} which may give rise to additional IR emission. Our models therefore assume that any material within R_{dust} is optically thin, which is a good approximation for low mass disks. For high mass disks the gas may be optically thick producing larger near-IR excesses.

2.3. *Adopted Circumstellar Dust Properties*

Recent modeling of HST images (Cotera et al. 2001) and the SED of HH30 IRS (Wood et al. 2001) indicates that the circumstellar dust size distribution extends to larger grain radii than typical ISM grains. This is in agreement with many other observations indicating grain growth within protoplanetary disks (e.g., Beckwith et al. 1990; Beckwith & Sargent 1991). This paper primarily investigates the effects of disk mass on the SED and adopts circumstellar dust properties that reproduce the HH30 IRS SED. The dust model (chemical composition, mathematical form for the size distribution, calculation of opacity and scattering parameters, etc) is described in Wood et al. (2001) and we only summarize the main features here. Specifically, we adopt, a size distribution

$$n(a) \ da = C_i \ a^{-p} \exp\left(-[a/a_c]^q\right) \ da \ , \qquad (2)$$

with $p = 3.5$, $q = 0.6$, $a_c = 50\mu$m, $a_{\min} = 0.01\mu$m, and $a_{\max} = 1$mm. The exponential scalelength, a_c, yields dust particle sizes extending up to and in excess of 50μm. Figure 1 shows the wavelength dependence of the opacity, scattering albedo, and Heyney-Greenstein phase function asymmetry parameter (Heyney & Greenstein 1941) for this size distribution.

Recent *Infrared Space Observatory* spectra of Herbig Ae/Be stars (e.g., Meuss et al. 2000; Chiang et al. 2001; van den Ancker et al. 2000) are now allowing the circumstellar dust chemistry to be studied. Because we adopt the dust properties of Fig. 1 for our simulations, we have not investigated the effects of different chemical compositions on the the resulting disk SEDs. How the circumstellar chemistry effects the SED is an interesting problem, but it is beyond the scope of this paper and we present models for different disk masses and the dust properties shown in Figure 1. In addition, our models do not include additional heating from transiently heated small grains (see the new radiation transfer code of Misselt et al. 2001) which is not important in the cooler Classical T Tauri stars considered in this paper.

2.4. *Energy Sources*

The energy input to the disk is from stellar photons and accretion luminosity liberated in the disk. As discussed in the previous section, we fix the disk structure for our radiation transfer simulations. Given the disk structure (Eq. 1), α disk theory determines the accretion rate for a given disk mass. Our parameterization of the disk density and accretion follows that presented in the review by Bjorkman (1997), apart from the term $\pm\sqrt{R_0/\varpi}$. The accretion rate and viscosity parameter, $\dot{M}$ and α_{disk}, are related to the disk parameters by

$$\dot{M} = \sqrt{18\pi^3} \, \alpha_{\mathrm{disk}} \, V_c \, \rho_0 \, h_0^3/R_\star \ , \qquad (3)$$

where the critical velocity $V_c = \sqrt{GM_\star/R_\star}$. The flux due to viscous disk accretion, $GM_\star\dot{M}/2R_\star$, is generated throughout the disk midplane region according to (Shakura & Sunyaev 1973, Lynden-Bell & Pringle 1974)

$$\frac{dE}{dA \, dt} = \frac{3GM_\star\dot{M}}{4\pi\varpi^3}\left[1 - \sqrt{\frac{R_\star}{\varpi}}\right] \ . \qquad (4)$$

For low mass disks, the heating due to accretion luminosity is negligible and stellar irradiation dominates the disk heating. In general we choose $\alpha_{\mathrm{disk}} = 0.01$ (Hartmann et al. 1998), but for the most massive disk we simulate this results in a very large accretion luminosity, $L_A > 0.8L_\star$. For this case α_{disk} is adjusted so that $L_A < 0.2L_\star$ in line with recent observational determinations of accretion luminosities in classical T Tauri stars (Hartmann et al. 1998).

3. MODEL RESULTS: SEDS, COLORS

The following models use $T_\star = 4000$K, $R_\star = 2R_\odot$, $R_{\mathrm{disk}} = 100$AU, and a distance of 500pc to the system.

3.1. *SED Evolution with Disk Mass*

Figure 2 shows the effect on the SED of changing the disk mass, but keeping the disk structure fixed to that of our fiducial model. The massive optically thick disks produce SEDs that resemble that of the Kenyon & Hartmann (1987) flared disk model, aside from differences (addition of scattered light to pole-on views and silicate features) due to our inclusion of a finite albedo and non-gray opacity. The most massive disk has a very large near-IR excess due to the large accretion luminosity present in this model. The model SEDs display the characteristic features present in other simulations: large infrared excess emission, flat spectrum sources at intermediate inclinations, and double peaked spectra (optical and far-IR peaks) for very large inclinations. At large inclinations, the optical peak is due to scattered starlight as the dense disk totally obscures the star and disk emission at short wavelengths.

Reducing the disk mass has the most dramatic effect at long wavelengths with the SED rapidly declining with decreasing mass. At short wavelengths the disk remains optically thick to stellar photons over a wide range of mass so the near-IR excess is not as sensitive to mass. Figure 4 presents our models again, with the three panels showing SEDs for the range of disk masses at a given inclination. These results show similar features to the models of Men'shchikov & Henning (1997, their Fig. 12) who presented SEDs for a range of optical depths in a spherical geometry with evacuated bipolar cones.

The *SIRTF* sensitivity limits show that at a distance of 500pc very low mass disks ($M_{\mathrm{disk}} \gtrsim 10^{-6}M_\odot$) are detectable out to a wavelength of 70μm. At 25μm *SIRTF* will be sensitive to photospheric flux levels at 500pc, thus allowing for the detection of even lower mass disks. Our overall conclusion from these simulations is that near-IR excesses detect disks while far-IR excesses can be used to study their mass.

3.2. *Color Evolution with Disk Mass*

Figure 4 shows the variation of colors with disk mass for $i < 60°$. At long wavelengths we use the simulated flux at 70μm and 160μm in forming the color and have not adopted any particular color system. The colors are fairly insensitive to inclination for $i < 60°$, but see §3.3 for color-color and color-magnitude diagrams that include highly inclined disks. For a passive disk with $M_{\mathrm{disk}} = 10^{-1}M_\odot$, $\Delta(K-L) \approx 0.7$, decreasing to a fairly constant $\Delta(K-L) \approx 0.4$ for $10^{-7}M_\odot \leq M_{\mathrm{disk}} \leq 10^{-3}M_\odot$. Larger $K-L$ colors arise in massive disks where accretion

luminosity is included, $\Delta(K-L) \approx 1$ for $M_{\rm disk} = 10^{-1}M_{\odot}$. In our models, less massive disks do not sustain large accretion rates (see §2.3) and the $K - L$ excess is due to reprocessing of starlight. For these disks, $K - L$ is fairly insensitive to mass as the disk remains optically thick in the near-IR for masses $M_{\rm disk} \gtrsim 10^{-7}M_{\odot}$. Therefore ground based near-IR observations are capable of detecting very low mass disks. Again, we emphasize that this is the mass of small ($\lesssim 50\mu$m) particles which dominate the near-IR opacity.

At longer wavelengths the SED decreases with decreasing disk mass and this is reflected in the other color indexes remaining relatively flat with disk mass until the disk becomes optically thin at the waveband under study. At the longest *MIPS* wavelength, 160μm, the $K - 160$ color shows a clear progression from the most massive to least massive disk.

3.3. *Color-Color and Color-Magnitude Diagrams*

Figure 5 shows color-color diagrams for our model disks assuming intrinsic stellar colors from Kenyon & Hartmann (1995, Table A5). When we include all disk inclinations there are degeneracies in the color-mass parameter space, with large viewing angles generally leading to redder colors. This result differs from other investigations (e.g., Lada & Adams 1992; Kenyon, Yi, & Hartmann 1996; Meyer, Calvet, & Hillenbrand 1997) which assumed the disk emission was proportional to $\cos i$, giving the bluest colors for edge-on viewing. More detailed radiation transfer modeling shows that a simple $\cos i$ scaling does not give the correct inclination dependence for flared disk models.

The effect of changing the disk mass is not very strong in the $(K - L)/(K - N)$ diagram for $M_{\rm disk} \gtrsim 10^{-6}M_{\odot}$, reflecting that at short wavelengths the disks remain optically thick over a wide range of mass. The disk masses separate out more clearly in the $(K - N)/(K - 70)$ diagram. Therefore color-color diagrams of large numbers of sources that compare near and far infrared colors provide a means of determining the range of disk masses within a cluster.

Figure 5 showed that inclination effects lead to a large spread in the location of different disk masses in the color-color diagrams. This leads to degeneracies in the location of different disk masses. However, Fig. 6 shows how color-magnitude diagrams can help in breaking the mass-inclination degeneracy. Placing all our disk models on color-magnitude diagrams shows that disks viewed at large inclinations occupy the lower righthand corners, i.e., highly inclined disks are faint and red.

4. SED AND COLOR DEPENDENCE ON OTHER DISK PROPERTIES

4.1. *Flat Disks*

The previous sections presented SEDs for disks which have the flaring parameters that fit HH30 IRS images and SED. However, other investigations indicate a variety of disk structures in Classical T Tauri stars (e.g., Kenyon & Hartmann 1987; Miyake & Nakagawa 1995; Chiang et al. 2001). To investigate the effects of flatter disks on SEDs and colors we repeated the simulations of Fig. 2 with a reduced scaleheight $h_0 = 0.003R_\star$ giving $h(100{\rm AU}) = 3$AU. The smaller scaleheight results in the disk intercepting less

stellar radiation (e.g., Kenyon & Hartmann 1987) and consequently smaller excesses and bluer colors than our models in § 3. For a given disk mass, the mm flux is unaltered, but the mid to far-IR emission is sensitive to the disk structure (Kenyon & Hartmann 1987; Chiang et al. 2001). The qualitative variation of the SEDs and colors with disk mass remains the same.

4.2. *Grain Growth*

In our models the dust size distribution does not change as the disk mass decreases. However, small dust grains may coagulate to form larger grains and rocks thereby altering the grain size distribution in the disk (e.g., Beckwith, Henning, & Nakagawa 2000). This will lead to changes in the wavelength dependence of the opacity. D'Alessio et al. (2001) investigated grain growth by keeping the disk mass constant and increasing the maximum grain size (effectively reducing the population of small grains) and changing the slope of the power law size distribution. For a slope $p = 3.5$, their SED models show the largest effects occur for $\lambda \gtrsim 20\mu$m, while for $p = 2.5$ (which puts more mass into larger particles) the SEDs are similar to ours in which the total disk mass decreases. SEDs arising from either a low mass disk or a massive disk with large grains may be distinguished with detailed SED modeling.

4.3. *Disk Radius*

Decreasing the disk radius, but keeping the mass constant results in a disk that is denser and optically thicker than our models of § 3. A smaller disk effectively removes cool material at large radii that provides the bulk of the long wavelength emission, yielding smaller far-IR and mm fluxes (e.g., Beckwith et al. 1990). The other effect of squeezing the disk into a smaller volume is an increase in the height above the midplane at which stellar photons are absorbed. This gives a geometrically thicker dust disk that can intercept more stellar photons, raising the near and mid-IR emission. The overall effects of a very small disk are to increase the wavelength at which the disk becomes optically thin yielding larger $K - L$ colors and a slower decline in the $K - 180$ color with decreasing mass. The larger optical depth for small disks will lower the minimum disk mass that may be detected from $K - L$ colors. Large radius disks give the opposite of these effects: less near and mid-IR, and more far-IR and mm emission.

4.4. *Inner Disk Holes and Non-homologous Disk Evolution*

In order to investigate general trends, we have presented a simple model for disk evolution of protoplanetary disks in which the mass decreases homologously with time. Real disks will be more complicated than this, with the disk radius growing, changes in the flaring parameters due to dust settling, and the possibility of accretion being terminated through the opening up of large inner disk holes and gaps, resulting in "inside-out" evolution. Current data does not provide much support for the existence of large holes in protoplanetary disks: if they do not show near-IR excesses, mid-IR and mm excesses are usually absent also (Stassun et al. 2001, Haisch, Lada & Lada 2001a), but there are some exceptions notably GM Aur (Koerner, Sargent, & Beckwith 1993). *SIRTF* should be able to distinguish

between low mass protoplanetary disks, whose mass has evolved homologously (without creating large inner holes), and disks which have evolved by creating large inner holes and thus directly test the inside-out disk clearing scenario.

Debris disks often exhibit large inner holes or a ring-like structure (e.g., Koerner et al. 1998; Jayawardhana et al. 1998; Schneider et al. 1999). However, debris disks are not likely to be protoplanetary disks that have evolved large inner holes. Debris disks are sufficiently old that the dust in them is not remnant protoplanetary material but instead is created and continually replenished by collisions between planetessimals formed previously in the disk. Moreover, protoplanetary disks which simply evolve from the inside out by clearing large inner holes (but otherwise maintaining their initial structure), will still contain large reservoirs of material in their outer regions and thus should be considerably more massive than debris disks.

5. COMPARISON TO OBSERVATIONS: DISK MASSES IN TAURUS-AURIGA

Observations at mm and radio wavelengths, where the disk is optically thin, provide the best probe of disk mass (e.g., Beckwith et al. 1990). When such data is not available our models show that far-IR, and in certain circumstances even mid-IR data, can provide another means of probing disk mass (if the disks are not too massive and optically thick). For example, Kenyon & Hartmann (1995) presented a compilation of optical through far-IR observations of Taurus-Auriga sources and noted a pronounced gap in the $K-N$ distribution between the bluest Class II and the reddest Class III sources. Figure 7 shows the $(K-L)/(K-N)$ color-color diagram for the Taurus-Auriga sources along with our face-on model colors for various disk masses. In the context of our models, the gap in the $K-N$ distribution corresponds to disks with $M_{disk} \lesssim 10^{-6} M_{\odot}$ and indicates that there are few circumstellar disks with masses between 10^{-6} and 10^{-8} $M_{\odot}$ in the Taurus-Auriga cloud (of course, this disk mass does not include rocks and planets). This, in turn, could be interpreted to indicate that once the disk mass falls below $\sim 10^{-6} M_{\odot}$ the timescale for clearing the remaining material in the inner ($\lesssim 5-10$AU) disk is very rapid.

6. SUMMARY

We have investigated the observational signatures of an evolutionary model in which the disk mass decreases homologously, but the disk structure and stellar parameters remain constant with time. Our main conclusions are:

- *Near-IR observations detect disks.* Disks remain optically thick in the near-IR over a wide range of disk mass resulting in measurable $K-L$ excesses for disks down to $M_{disk} \sim 10^{-7} M_{\odot}$. This corresponds to a dust mass of $M_{dust} \sim 10^{-9} M_{\odot}$.

- *Mid-IR observations probe disk structure.* Observations in the 20μm $\lesssim \lambda \lesssim 100\mu$m range are sensitive to the disk flaring parameters and are crucial for determining the degree of dust settling.

- *Far-IR most sensitive to disk mass.* The far-IR emission decreases rapidly with disk mass resulting in a strong correlation between $K-160$ and disk mass. Our simulations indicate that at a distance of 500pc, *SIRTF* will be able to detect $M_{disk} \gtrsim 10^{-6} M_{\odot}$ with a 500s exposure at 70μm and even lower masses at 25μm.

- *General trends are reproduced for a range of disk parameters.* Despite degeneracies in fitting SEDs of particular sources, we find that varying the disk parameters within generally accepted limits introduces a spread in the color-mass relationship, but does not affect the general trends.

The degeneracies inherent in fitting disk models to wavelength restricted datasets illustrates that it is necessary to have full SED coverage to constrain the disk structure and dust size distribution (e.g., Men'shchikov & Henning 1997; Chiang et al. 2001; D'Alessio et al. 2001). *SIRTF, SMA,* and *ALMA* will provide detailed SEDs for nearby sources enabling detailed modeling of the disk mass and structure. For studies of stellar clusters, such data will not be available and mm observations, which are most sensitive to disk mass, cannot as yet achieve the required sensitivity and resolution to study low mass disks and/or distant clusters. Therefore, we must appeal to statistics and determine average properties of sources in different clusters for studying disk evolution. *SIRTF* will provide broad band colors for hundreds of sources within a given cluster, from which we can construct median colors and the spread around the median for each cluster (e.g., Haisch, Lada, & Lada 2001b). From our models it is apparent that NIR excesses detect disks, and therefore the absence of a $K-L$ excess within a cluster of a given age can determine the maximum disk lifetime. By comparing the median colors from different clusters with a spread in age (as a whole and as functions of position within the cluster), we can search for trends as a function of cluster age. Therefore, the far-IR probed by *SIRTF* may allow us to determine a timescale for disk evolution — i.e., in our homologous evolutionary model we would be able to convert the color-mass correlation to one which tracks disk mass in clusters as a function of age, analogous to the recent *ISO* analysis of debris disks by Spangler et al. (2001).

REFERENCES

Adams, F.C., Emerson, J.P., & Fuller, G.A. 1990, ApJ, 357, 606
Adams, F.C., Lada, C.J., & Shu, F.H. 1987, ApJ, 308, 788
Adams, F.C., & Shu, F.H. 1986, ApJ, 308, 836

Backman, D.E., & Paresce, F. 1993, in Protostars and Planets III, ed. E.H. Levy & J.I. Lunine (Tuscon: Univ. Arizona Press), 1253

Beckwith, S. V. W., Henning, T., & Nakagawa, Y. in "Protostars and Planets IV," eds Mannings, V., Boss, A.P.,& Russell, S. S., (Tucson: University of Arizona Press), 533

Beckwith, S.V.W., & Sargent, A.I. 1993, in Protostars & Planets III, ed. E.H. Levy & J.I. Lunine (Tucson: Univ. Arizona), 543

Beckwith, S.V.W., & Sargent, A.I. 1991, ApJ, 381, 205

Beckwith, S.V.W., Sargent, A.I., Chini, R.S., & Gusten, R. 1990, AJ, 99, 924

Bell, K.R. 1999, ApJ, 526, 411

Bell, K.R., Cassen, P.M., Klahr, H.H., & Henning, T. 1997, ApJ, 486, 372

Bjorkman, J.E., & Wood, K. 2001, ApJ, 554, 615

Bjorkman, J.E. 1997, in "Stellar Atmospheres : Theory and Observations," eds J.P. De Greve, R. Blomme, & H. Hensberge (Springer)

Boss, A.P., & Yorke, H.W. 1996, ApJ, 469, 366

Burrows, C.J., et al. 1996, ApJ, 473, 437

Calvet, N., Canto, J., Binette, L., & Raga, A.C. 1992, Rev. Mex., 24, 81

Chiang, E.I., Joung, M.K., Creech-Eakman, M.J., Qi, C., Kessler, J.E., Blake, G.A., & van Dishoeck, E.F. 2001, ApJ, 547, 1077

Chiang, E.I., & Goldreich, P. 1999, ApJ, 519, 279

Chiang, E.I., & Goldreich, P. 1997, ApJ, 490, 368

Cohen, M., & Kuhi, L.V. 1979, ApJS, 41, 743

Cotera, A.S., et al. 2001, ApJ, 556, 958

D'Alessio, P., Calvet, N., & Hartmann, L. 2001, ApJ, 553, 321

D'Alessio, P., Calvet, N., Hartmann, L., Lizano, S., & Canto, J. 1999, ApJ, 527, 893

D'Alessio, P., Canto, J., Calvet, N., & Lizano, S. 1998, ApJ, 500, 411

Dutrey, A., Guilloteau, S., Duvert, G., Prato, L., Simon, M., Schuster, K., & Menard, F. 1996, A&A, 309, 493

Efstathiou, A., & Rowan-Robinson, M. 1991, MNRAS, 252, 528

Grady, C.A., et al. 2000, ApJ, 544, 895

Haisch, K.E., Lada, E.A., & Lada, C.J. 2001a, AJ, 121, 2065

Haisch, K.E., Lada, E.A., & Lada, C.J. 2001b, ApJ, 553, L153

Haisch, K.E., Lada, E.A., & Lada, C.J. 2000, AJ, 120, 1396

Hartmann, L., Calvet, N., Gullbring, E., & D'Alessio, P. 1998, ApJ, 495, 385

Henyey, L.C., & Greenstein, J.L. 1941, ApJ, 93, 70

Hillenbrand, L.A., Strom, S.E., Vrba, F.J., & Keene, J. 1992, ApJ, 397, 613

Jayawardhana, R., Fisher, S., Hartmann, L., Telesco, C., Pina, R., & Razio, G. 1998, ApJ, 503, L79

Kenyon, S.J., Yi, I., & Hartmann, L. 1996, ApJ, 462, 439

Kenyon, S.J., & Hartmann, L. 1995, ApJS, 101, 117

Kenyon, S.J., & Hartmann, L. 1987, ApJ, 323, 714

Kim, S.H., Martin, P.G., & Hendry, P.D. 1994, ApJ, 422, 164

Koerner, D.W., Ressler, M.E., Werner, M.W., & Backman, D.E. 1998, ApJ, 505, L83

Koerner, D.W., & Sargent, A.I. 1995, AJ, 109, 2138

Koerner, D.W., Sargent, A.I., & Beckwith, S.V.W. 1993, ApJ, 408, L93

Koresko, C.D. 1998, ApJ, 507, L145

Krist, J.E., Stapelfeldt, K.R., Menard, F., Padgett, D.L., & Burrows, C.J. 2000, ApJ, 538, 793

Lada, C.J., & Adams, F.C. 1992, ApJ, 393, 728

Lynden-Bell, D., & Pringle, J.E. 1974, MNRAS, 168, 603

Mendoza, E.E. 1968, ApJ, 151, 977

Men'shchikov, A.B., & Henning, T. 1997, A&A, 318, 879

Meyer, M.R., Calvet, N., & Hillenbrand, L.A. 1997, AJ, 114, 288

Miyake, K., & Nakagawa, Y. 1995, ApJ, 441, 361

O'Dell, C.R., Wen, Z., & Hu, X. 1993, ApJ, 410, 696

Padgett, D.L., Brandner, W., Stapelfeldt, K.R., Strom, S.E., Terebey, S., & Koerner, D.W. 1999, AJ, 117, 1490

Roddier, C., Roddier, F., Northcott, M.J., Graves, J.E., Jim, K. 1996, ApJ, 463, 326

Rucinski, S.M. 1985, AJ, 90, 2321

Rydgren, A.E., Strom, S.E., & Strom, K.M. 1976, ApJS, 30, 307

Shakura, N.I., & Sunyaev, R.A. 1973, A&A, 24, 337

Schneider, G., et al. 1999, ApJ, 513, L127

Shu, F.H., Adams, F.C., & Lizano, S. 1987, ARA&A, 25, 23

Sonnhalter, C., Preibisch, T., & Yorke, H.W. 1995, A&A, 299, 144

Spangler, C., Sargent, A.I., Silverstone, M.D., Becklin, E.E., & Zuckerman, B. 2001, ApJ, in press, astro-ph/0103185

Stapelfeldt, K. R., & Moneti, A. 1999 in "The Universe as Seen by ISO", Eds. P. Cox & M. F. Kessler, ESA-SP 427, 521

Stapelfeldt, K. R., Krist, J.E., Menard, F., Bouvier, J., Padgett, D.L., & Burrows, C.J. 1998, ApJ, 502, L65

Stassun, K.G., Mathieu, R.D., Vrba, F.J., Mazeh, T., & Henden, A. 2001, AJ, 121, 1003

Thi, W.F., et al. 2001, Nature, 409, 60

Wilner, D., & Lay, O. 2000, in "Protostars and Planets IV," eds Mannings, V., Boss, A.P.,& Russell, S. S., (Tucson: University of Arizona Press), p. 509

Wolf, S., Henning, T., & Stecklum, B. 1999, A&A, 349, 839

Wood, K., Wolff, M.J., Bjorkman, J.E., & Whitney, B.A. 2001, ApJ, in press, astro-ph/0109048
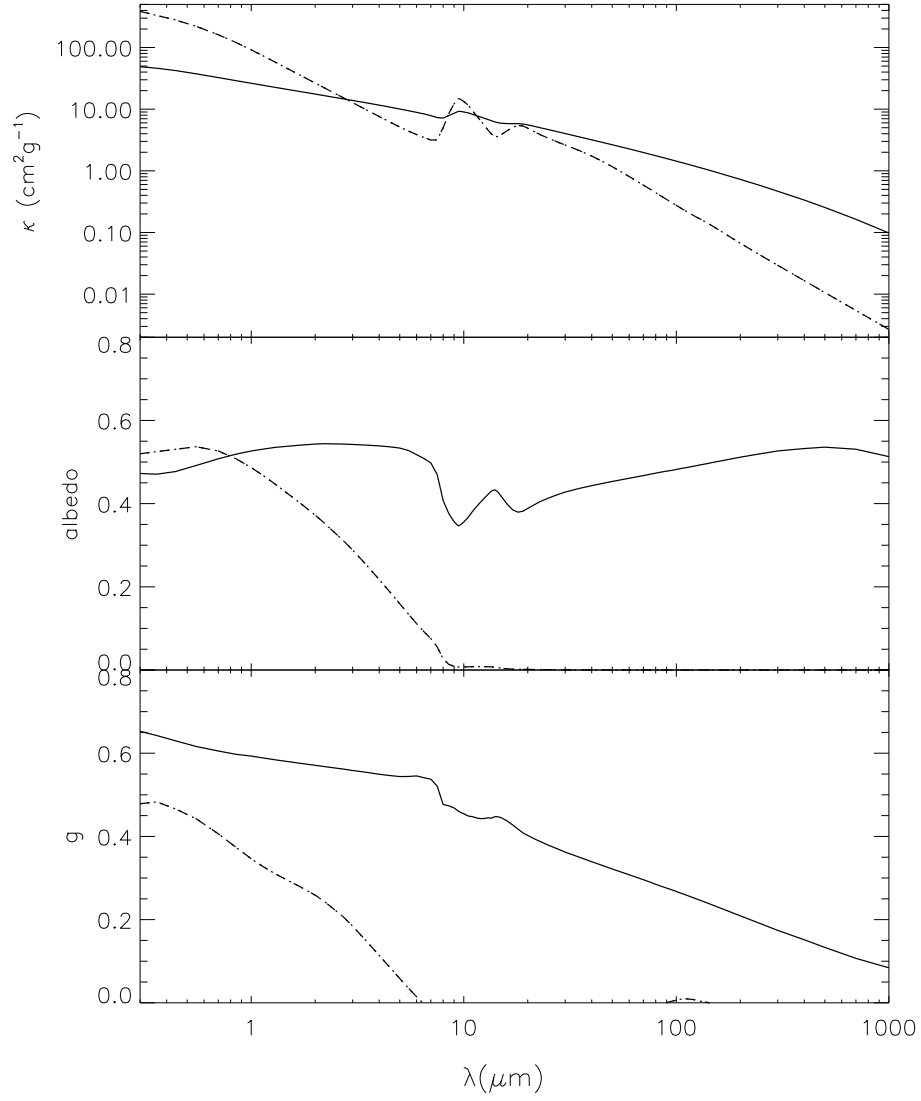
FIG. 1.— Dust parameters for a grain size distribution that fits the scattered light images and SED of HH30 IRS (solid line). The dashed lines show ISM grain parameters (Kim, Martin, & Hendry 1994). The three panels show total opacity (upper), albedo (middle), and cosine asymmetry parameter (lower).
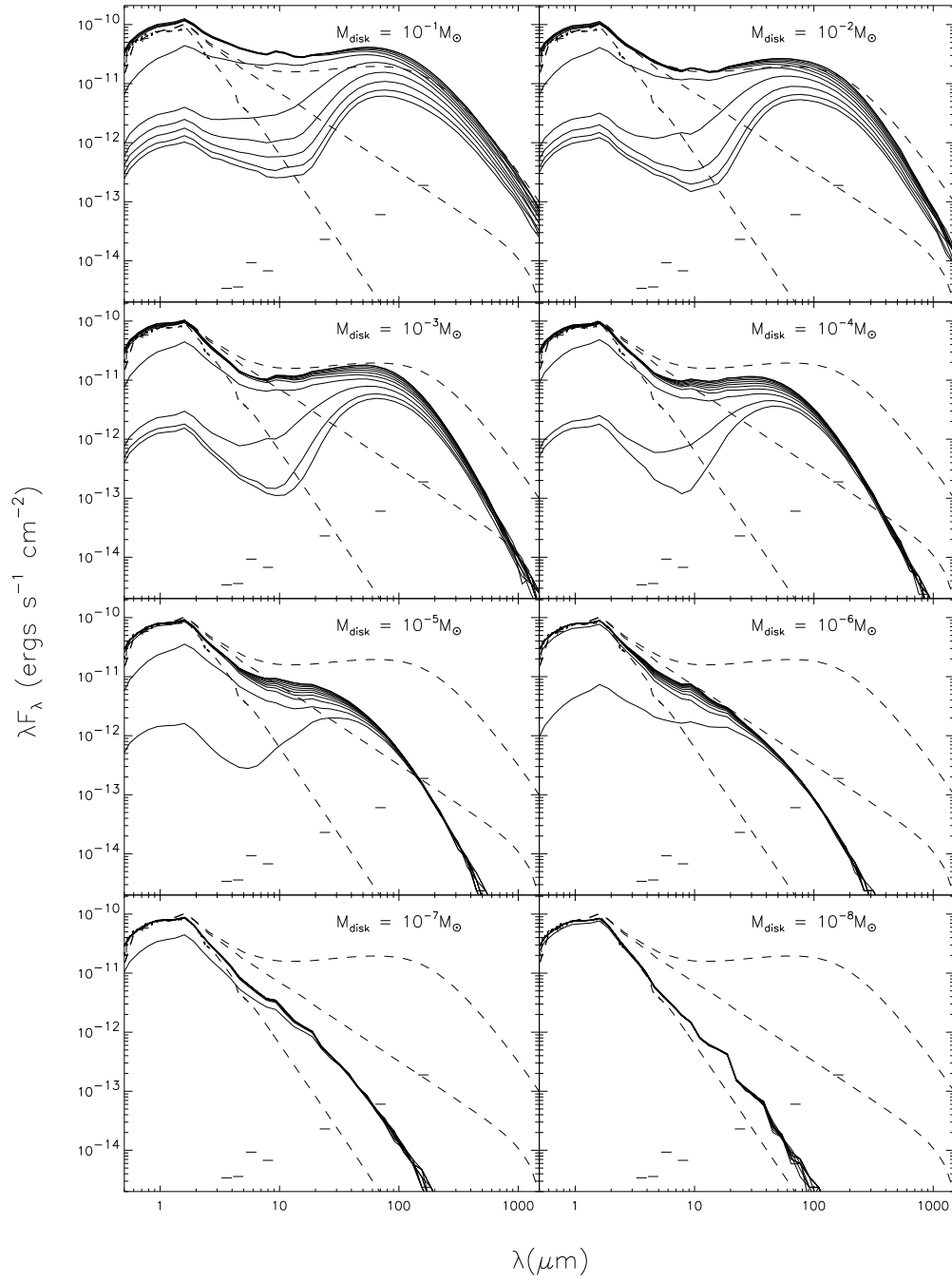
FIG. 2.— Evolution of SED with disk mass. Each panel shows model SED at ten viewing angles (evenly spaced in $\cos i$), ranging from $i = 87°$ (lowest curve) to $i = 13°$ (upper curve). Also shown are the input stellar spectrum and optically thick flat and flared reprocessing disk models. The star is assumed to be at a distance of 500 pc. The short horizontal lines are 5σ *SIRTF* sensitivity limits for a 500 s exposure (http://sirtf.jpl.nasa.gov/SSC/B_Observing/SSC_B2.html).
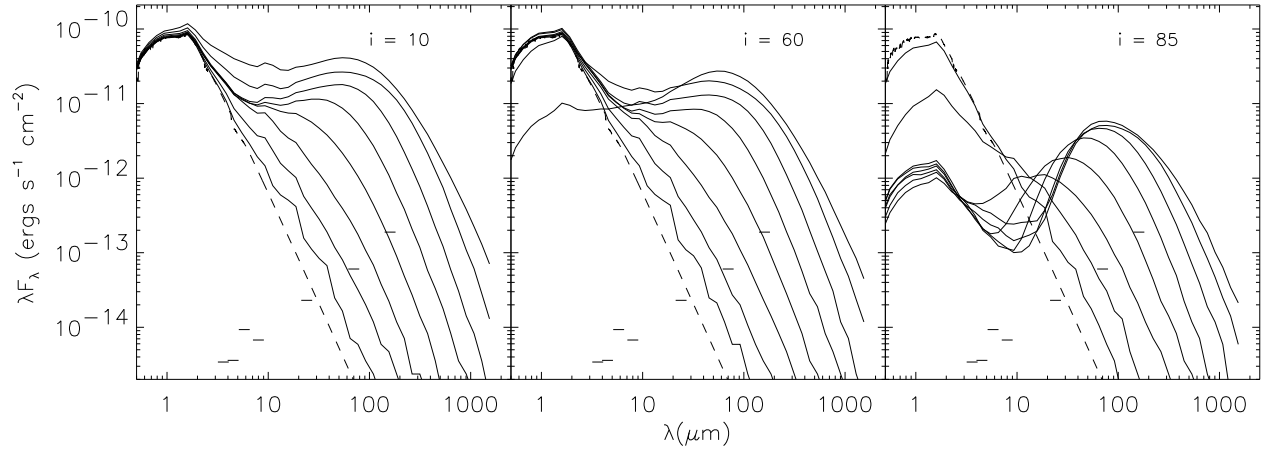
FIG. 3.— Evolution of SED with disk mass. Each panel shows model SEDs for a fixed viewing angle for the range of disk masses, $M_{\rm disk} = 10^{-8} M_{\odot}$ (lowest curve) to $M_{\rm disk} = 10^{-1} M_{\odot}$ (upper curve). Input spectrum and *SIRTF* sensitivities are as in Fig. 3.
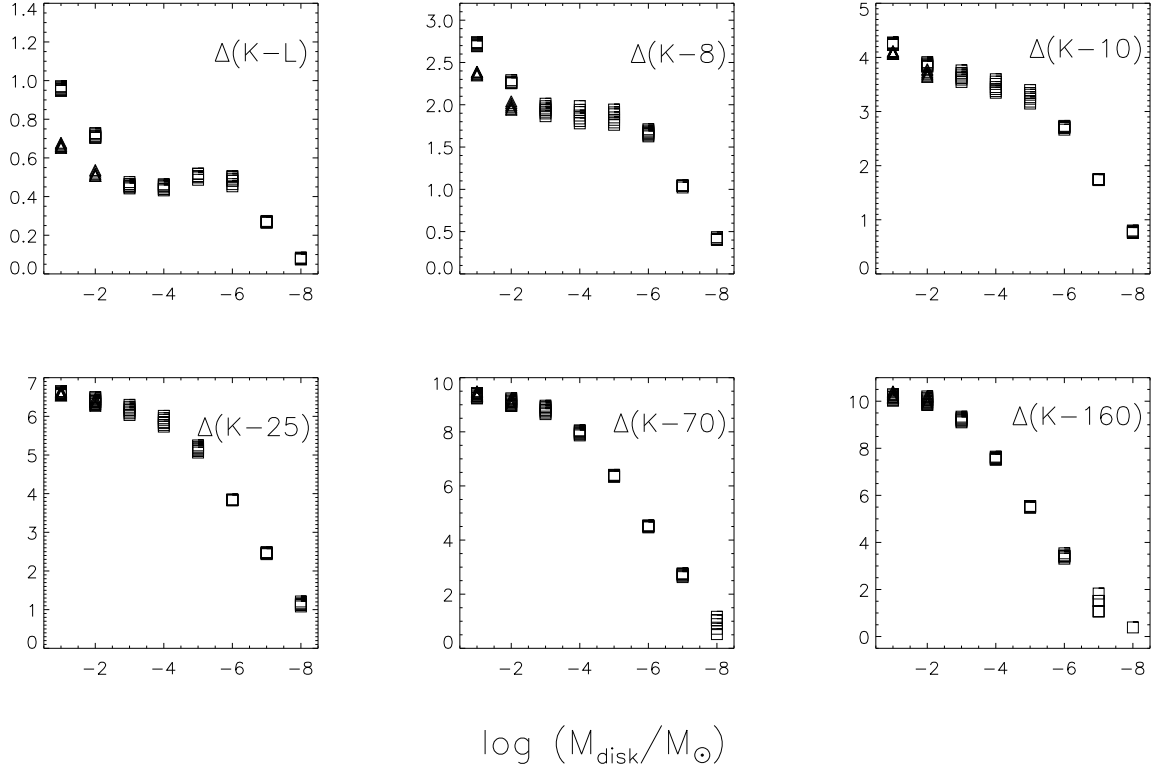
FIG. 4.— Colors as a function of disk mass for inclinations $i < 60°$. Triangles are passive disks, squares include accretion luminosity. This bottom panels show that long wavelengths are more sensitive to disk mass.

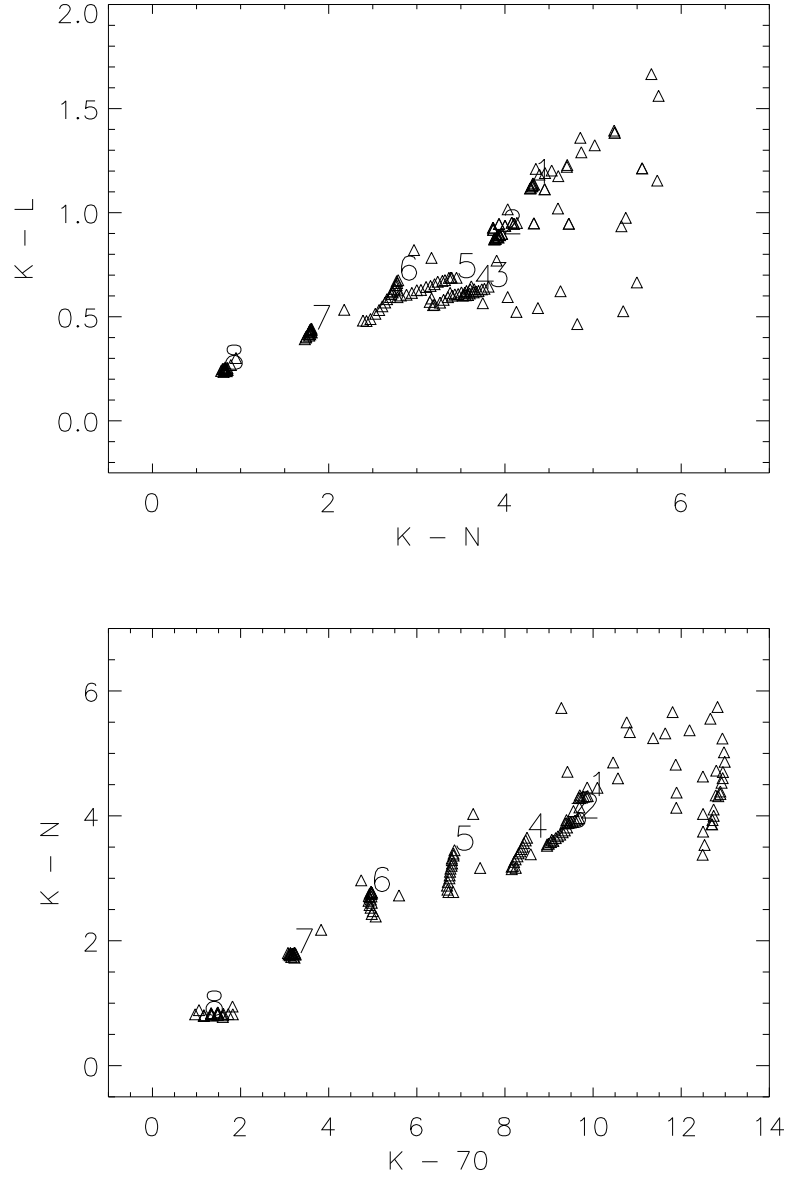

FIG. 5.— Color-color diagrams for our models. For each model we show twenty inclinations, evenly spaced in $\cos i$. The numbers are the locations of different mass disks viewed pole on, $10^{-1} M_\odot = 1$, $10^{-2} M_\odot = 2$, $10^{-3} M_\odot = 3$, etc. The very red colors are the highly inclined disks. As with Fig. 4, the bottom panel shows that long wavelength colors can distinguish a wide range of disk masses.
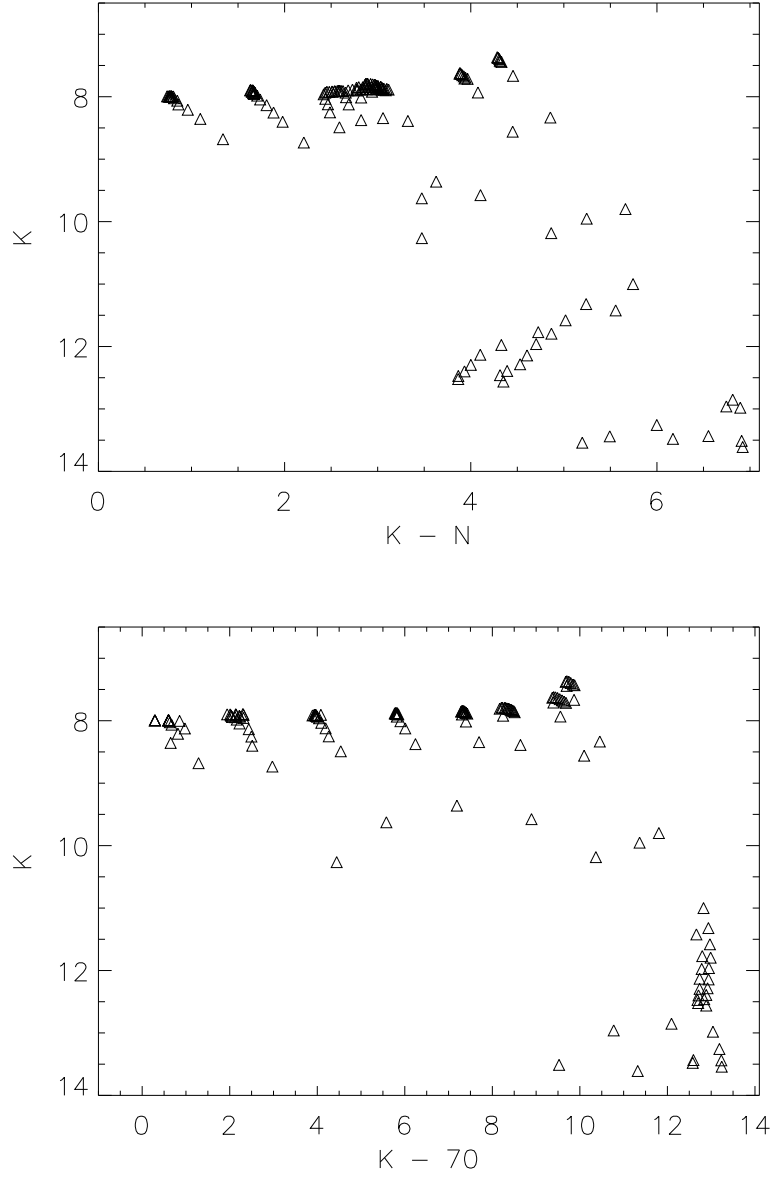
Fig. 6.— Color-magnitude diagrams for our models assuming a distance of 500pc. The edge-on disk sources are very faint and red and occupy the lower right corners of the color-magnitude diagrams.
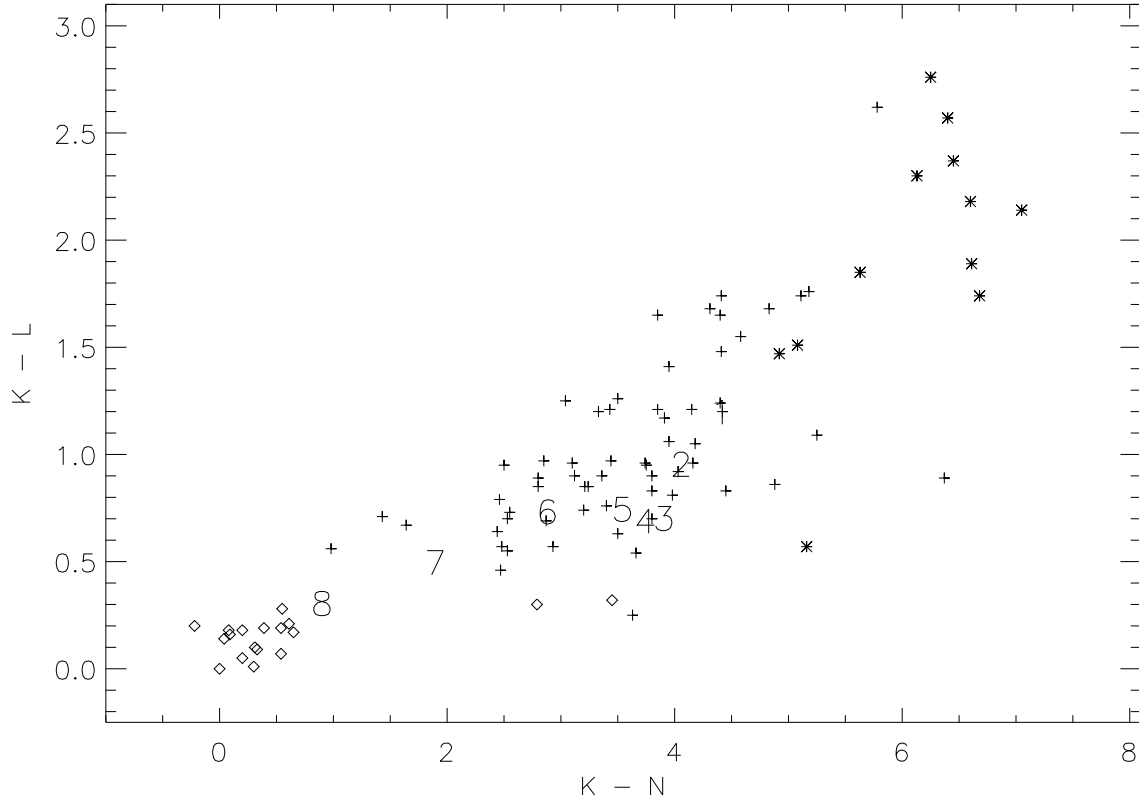
Fig. 7.— Color-color diagrams for Taurus-Auriga sources Class III (diamonds), Class II (crosses), Class I (stars). The data are taken from the Kenyon & Hartmann (1995) compilation. The numbers are our models for different mass disks viewed pole-on as in Fig. 5. The gap in the $K - N$ distribution between the Class II and Class III sources is filled in by our models having $M_{\rm disk} \lesssim 10^{-6} M_\odot$, which may imply that the timescale to clear $M_{\rm disk} \lesssim 10^{-6} M_\odot$ is very rapid.